Lawrence Berkeley National Laboratory
Recent Work

Title
COAL LIQUEFACTION RESEARCH

Permalink
https://escholarship.org/uc/item/85h5k1bf

Author
Heinemann, H.

Publication Date
1981-09-01

eScholarship.org Powered by the California Digital Library
University of California

LBL-13238
UC-90d

Lawrence Berkeley Laboratory
UNIVERSITY OF CALIFORNIA

Materials & Molecular Research Division

SEP 25 1981

COAL LIQUEFACTION RESEARCH

Heinz Heinemann

September 1981

TWO-WEEK LOAN COPY

This is a Library Circulating Copy which may be borrowed for two weeks. For a personal retention copy, call Tech. Info. Division, Ext. 6782

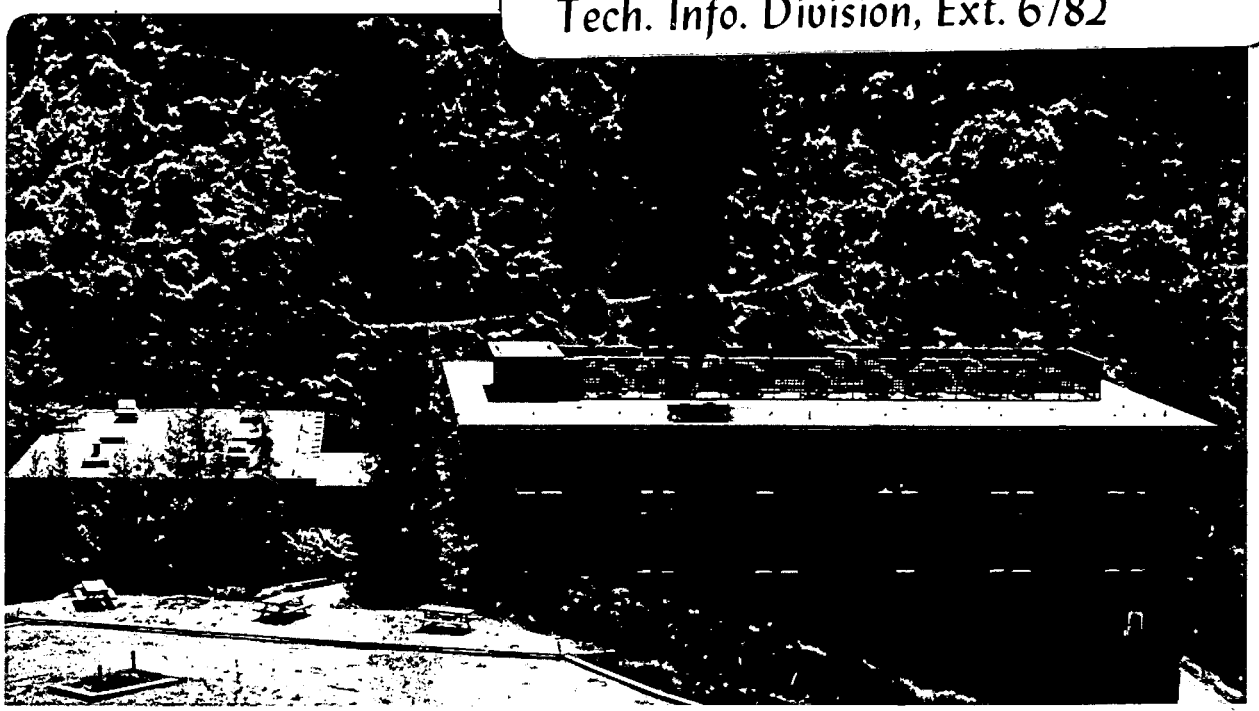

Prepared for the U.S. Department of Energy under Contract W-7405-ENG-48

LBL-13238

DISCLAIMER

This document was prepared as an account of work sponsored by the United States Government. While this document is believed to contain correct information, neither the United States Government nor any agency thereof, nor the Regents of the University of California, nor any of their employees, makes any warranty, express or implied, or assumes any legal responsibility for the accuracy, completeness, or usefulness of any information, apparatus, product, or process disclosed, or represents that its use would not infringe privately owned rights. Reference herein to any specific commercial product, process, or service by its trade name, trademark, manufacturer, or otherwise, does not necessarily constitute or imply its endorsement, recommendation, or favoring by the United States Government or any agency thereof, or the Regents of the University of California. The views and opinions of authors expressed herein do not necessarily state or reflect those of the United States Government or any agency thereof or the Regents of the University of California.

FINAL REPORT

Coal Liquefaction Research

October 1, 1978 - September 30, 1981

Grant No. ET-78-G-01-3425

Principal Investigator: Heinz Heinemann

Lawrence Berkeley Laboratory
University of California
Berkeley, CA 94720

This work was supported by the Assistant Secretary of Fossil Energy, Office of Coal Research, University Contracts Division of the U. S. Department of Energy under Contract No. W-7405-ENG-48.

INDEX

Summary	Page
Introduction	2
Section I, Catalytic Cracking with Water-wet Silica-Alumina Catalysts	3
A) Background	3
B) Work Hypothesis	7
C) Work performed and discussion	7
D) Conclusions	12
E) References	12
Section II, Fischer-Tropsch Reactor Studies	14
A) Background	14
B) Work Hypothesis	16
C) Work performed and Discussion	16
1) Fixed Bed Reactors	16
i) Equipment	17
ii) Experimental Procedure	17
iii) Results	18
iv) Conclusions	25
v) References	26
2) Slurry Reactor	28
i) Introduction	28
ii) Work Performed and Nomenclature	29
a) Experimental Work	31
b) Reactor Model	40
α Parameter Estimation	42
β Numerical Methods	44
c) Results and Discussion	46
iii) Conclusions	61
iv) References	62

INTRODUCTION

The Principal Investigator received a DOE, Fossil Energy, "Distinguished Scientist/Engineer" grant in the summer of 1978 at the time of his move to the Lawrence Berkeley Laboratory, University of California, Berkeley, after 40 years of industrial research. The grant was much appreciated because it enabled him to start a first research program at the new institution. The present final report of work performed under this three-year grant comprises research carried out jointly with Professor A. T. Bell and two graduate students, W. G. McKee and David Stern, whose collaboration is gratefully acknowledged.

The original proposal work on which is reported in the first section of this report was found to be based on an assumption which turned out not to be valid. However, some surprising observations were made.

A brief exploratory effort was simultaneously undertaken to test a hypothesis that coal and in particular lignite consist essentially of polymerized lignin and that it should be possible to dissolve lignite in liquors identical or similar to those used in paper pulping. While promising, this approach was dropped when the P.I. learned of successful research along these lines in industry.

With the agreement of the DOE program administrator, research during the last two years of the contract concentrated on Fischer-Tropsch synthesis and particularly on similarities and differences between fixed bed and slurry-type reactors. This is described in the second section of the report.

The work has resulted in three issued and pending publications,[1] as well as a "Master of Science" thesis. It has opened up new leads which will hopefully be explored in the future.

SECTION I

Catalytic Cracking With Water-Wet Silica-Alumina Catalysts

A) Background

An understanding of the chemistry of catalytic cracking must be based on knowledge of the structure of the silica-alumina type catalysts used in this work and on the generally accepted mechanism of catalytic cracking.

The basic building block of both amorphous and crystalline (zeolitic) silica-alumina catalysts can be envisioned as silica (1):

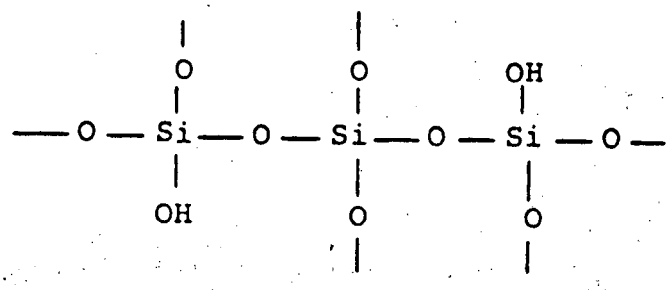

which, if allowed to polymerize in an aqueous solution, forms a hydrogel. This gel alone is catalytically inactive, but if treated with an aluminum salt, Bronsted acid sites are formed as seen in Figure 1 (2):

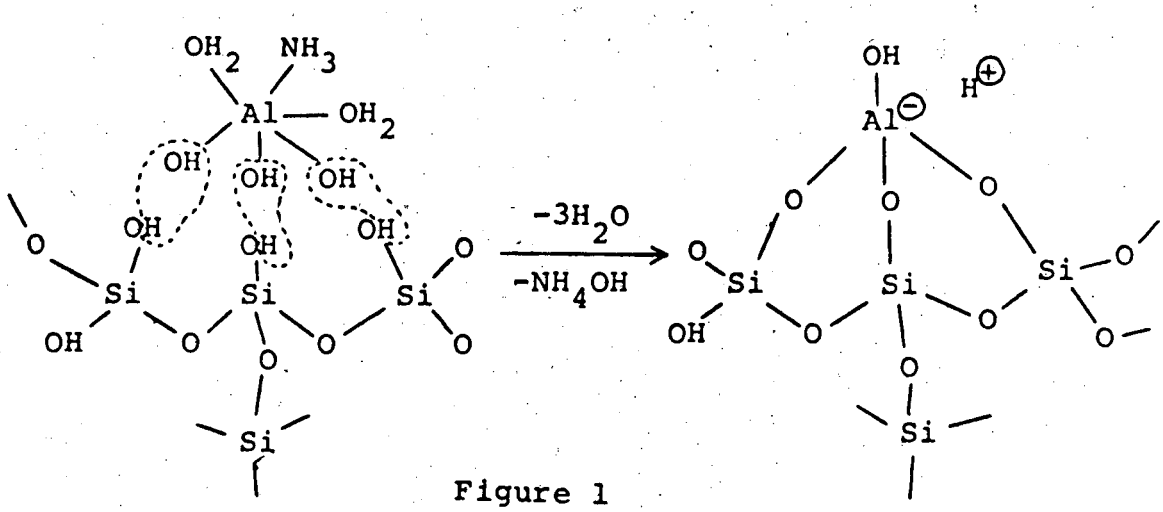

Figure 1

Upon heating, Bronsted acid sites can be converted to Lewis acid sites through the elimination of water as seen in Figure 2 (2):

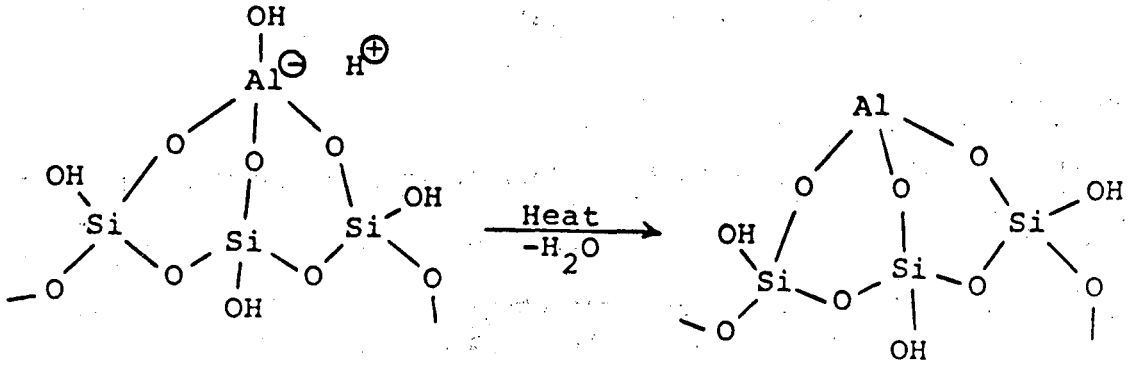

Figure 2

Depending on the degree of heat treatment (calcination), the catalyst surface will, therefore, exhibit varying amounts of both Bronsted and Lewis acid characteristics.

A different catalyst structure has been proposed by C. L. Thomas (1, 3). In this case the aluminum ion is attached by three-quarter strength covalent bonds to four oxygen atoms. This satisfies the trivalent nature of aluminum, but leaves each oxygen atom one quarter valence short, and since it is a negative valence there is a net negative charge. Balancing this charge, then, is a proton creating a Bronsted site which cannot easily be removed by calcination. (Figure 3)

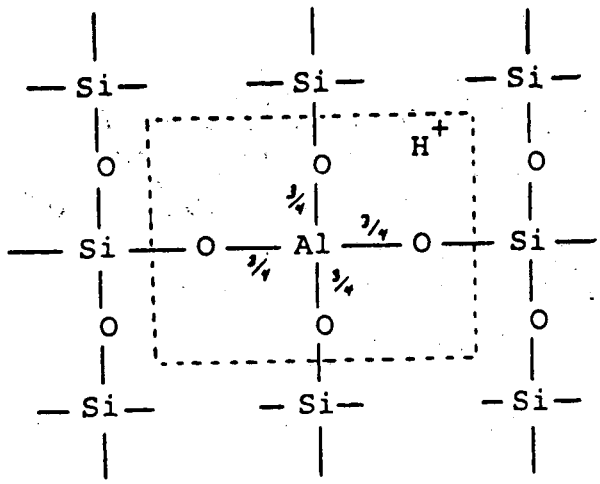

Figure 3

Mechanisms for catalytic cracking have been discussed in detail in numerous articles (1, 4-9). It is generally concluded that carbonium ions are responsible for the bulk of reactions which are involved in catalytic cracking. It is clearly the acid nature of the catalyst which initiates carbonium ion formation, but it has long been debated whether it is the Lewis or Bronsted sites which are most essential for this function. The Bronsted acid has the ability to donate a proton to the double bond of an olefin, while the Lewis acid may be able to abstract a hydride ion from paraffinic hydrocarbons achieving the same result. These differences become more evident in the following reactions:

Cracking of olefins: The first step of the mechanism involves the creation of a cation site. This is achieved by a direct attack of the Bronsted proton on the double bond:

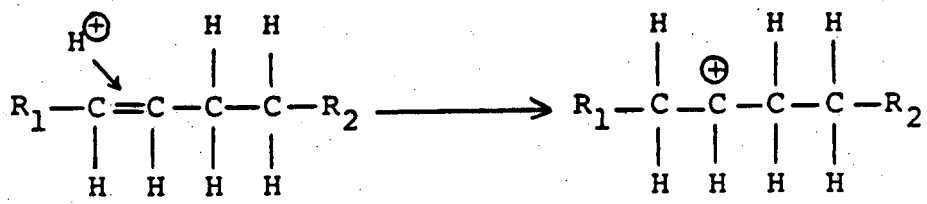

After the creation of the activated molecule, a breakage of the carbon-carbon bond can occur. This will always occur as a beta scission (10), creating an olefinic product and a new primary carbonium ion:

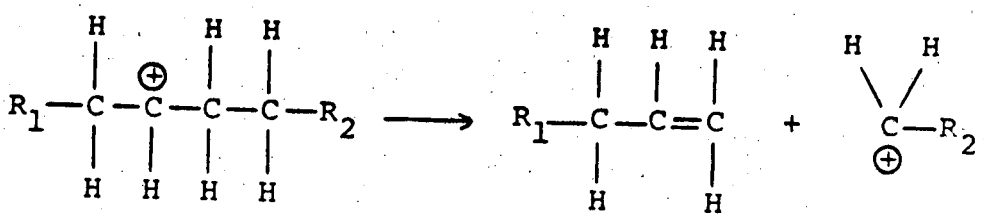

According to Markovinikov's rule (3), the new carbonium ion will undergo hydride and methyl group shifts to form a more stable cation. This rearrangement is what creates favorable isomerization toward a higher quality gasoline.

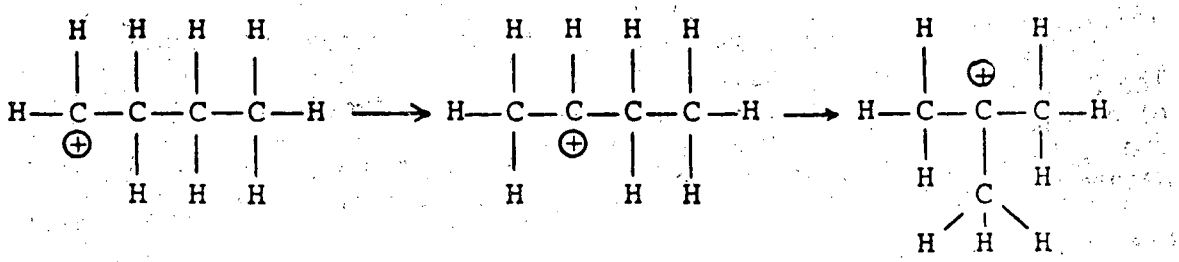

Termination may occur in one of two ways. The carbonium ion can abstract a hydride ion from a paraffin, forming both a paraffinic product and a new carbonium ion; or it may return a proton directly to the catalyst, creating both an olefinic product and an acid site. A large portion of the hydrogen necessary to form paraffins is obtained from "coke" formation--olefinic polymerization into large aromatic networks.

Cracking of Paraffins: Paraffins crack at a significantly slower rate than olefins, since there are no pi electrons for an acidic proton to attack. Again there are several mechanistic possibilities. It is feasible that a hydride ion is abstracted to form molecular hydrogen with a Bronsted proton, or withdrawn by the attraction of a Lewis acid site. It is also possible that olefins are present as impurities, or as a result of thermal cracking, allowing the mechanism to proceed as previously shown. In fact, it has been demonstrated that by adding small amounts of olefins to paraffin reactants, the rate of cracking can be accelerated significantly (3,4,11).

Hansford (12) summarizes the cracking mechanism as follows:

1) The mechanism is certainly ionic, and the carbonium ion theory gives an excellent accounting for differences in thermal and catalytic cracking.

2) It is probable, but not proven that the mechanism is a chain reaction for saturated hydrocarbons with an uncertain initiation step. The strongest evidence indicates that olefinic impurities are necessary to start the reaction, although hydride abstraction may occur simultaneously. A chain mechanism is not necessary to explain cracking of olefins.

3) Hydrogen transfer between olefins and saturates is not well understood, but it has been proposed that an olefin-catalyst complex may be able to abstract hydride ions.

4) High protonic activity seems to be well correlated with high catalyst activity for silica-alumina catalysts.

B) Work Hypothesis

The addition of liquid water to amorphous and possibly also crystalline silica-alumina cracking catalysts may enhance the catalytic activity and/or selectivity by increasing the number of Bronsted acid sites. Increased activity would permit cracking to occur at lower temperatures, which would be particularly valuable in the cracking of coal liquids.

C) Work Performed and Discussion

The cracking of n-hexadecane was investigated with four catalysts at very low temperatures, both in the presence and absence of liquid water.

It was determined that cracking could be observed in all cases at 250°C, a temperature considerably below that at which it is normally expected to occur. While the amounts of cracked product were very small (1-1.5% conversion), they were sufficient for gas chromatographic analysis.

Catalysts used in this work were:

(1) Davison Chemical Company silica-alumina, 35 activity index fluid bed catalyst, SMR 5-1721, 25% Al_2O_3 DR #498 A-D Davison Index 19*

(2) Houdry Process Corporation silica-alumina crushed pellets, 46 activity index #36 D2-54Z (HSA-300).

(3) Davison Chemical Company FCC catalyst (zeolite) SMR 5-1721 CBZ-1.

(4) Mobil Oil Corporation Durabead 9, crushed pellets (zeolite) Reference No. TE-15029.

Experimental work was carried out in a stirred glass flask, containing the n-hexadecane, catalyst, and, in some cases, water. Ten grams of catalyst, 15 g of hydrocarbon, and 1 g of water were used. The flask was immersed in an oil bath and heated at 250°C for 1 hr. A condenser was connected to the flask, and at the end of each experiment the overhead product was returned to the flask contents, which were then sampled and analyzed. Prior to use, all catalysts were calcined in dry air at 500°C, and if water was to be added, it was added dropwise while shaking the flask. The contents were then permitted to equilibrate in an inert atmosphere for 24 hrs at room temperature before adding the hydrocarbon.

In all cases, the presence of water reduced catalyst activity. In all but one case, product distributions were nearly identical. Liquid products ranged from C_4 to C_{15}, with a paraffin/olefin ratio of 1:2 and a branched/straight chain ratio of 1:2. In the case of one catalyst (catalyst 1 above), the product distribution was radically altered in the presence of water, indicating a change in the cracking mechanism. In this case

* Composition of This Catalyst is Shown in Table 1

Table 1

CHEMICAL AND PHYSICAL ANALYSIS OF THE

AI-35 DAVISON CATALYST

CHEMICAL ANALYSIS		PHYSICAL ANALYSIS	
T. V. @ 1750°F	11.99	0 - 20 microns	2%
% Silica (SiO_2)	74.54	0 - 40 microns	18%
% Alumina (Al_2O_3)	24.92	0 - 80 microns	75%
% Sodium (Na_2O)	.031	0 - 105 microns	89%
% Iron (Fe)	.028	0 - 149 microns	99%
% Sulfate (SO_4)	.48		
		A.P.S.	62 microns

Davison index	19
Jersey index	2.0

A..B.D.	.44
P.V.	.78
M.A. @ 1350	41.19
CF	.85
GF	1.33

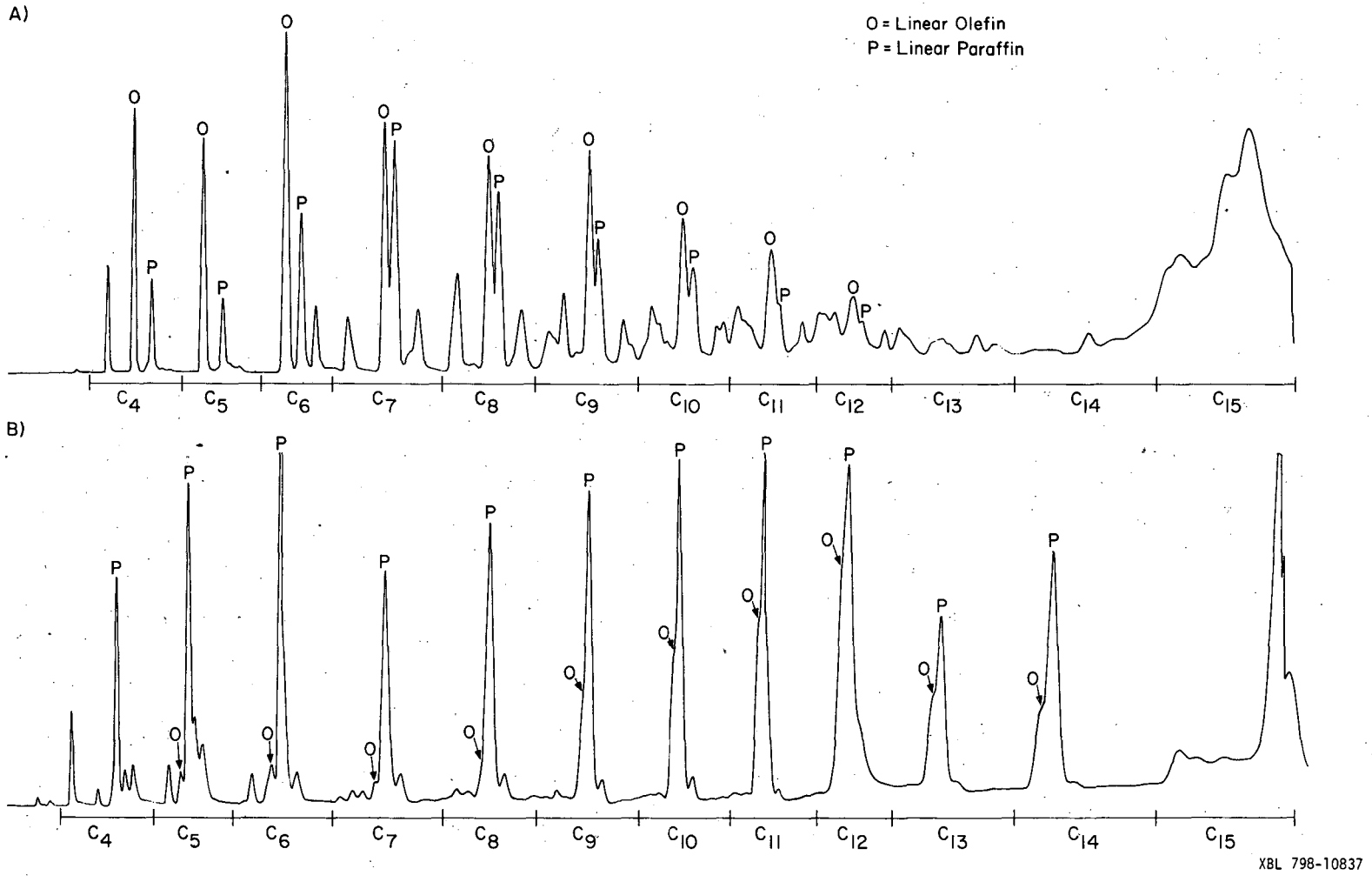
A)
O = Linear Olefin
P = Linear Paraffin
B)
C4
C5
C6
C7
C8
C9
C10
C11
C12
C13
C14
C15
XBL 798-10837

Figure 1

TABLE 2

SUMMARY OF CRACKING RUNS

RUN #	CATALYST	ADDITIVE	TIME MIN.	CONVERSION* %	DISTRIBUTION	COMMENTS
1	Durabead 9	10% H_2O	30	-	"Normal"	
2	Durabead 9	10% H_2O	30	.05	"Normal"	Total reflux
3	Durabead 9	None	30	.50	"Normal"	Total reflux
4	AI-35 Davison	None	60	1.0	"Normal"	Total reflux
5	AI-35 Davison	10% H_2O	60	.10	Paraffinic	Total reflux
6	AI-35 Davison	10% H_2O	60	.15	Paraffinic	No reflux
7	AI-35 Davison	None	60	1.0	"Normal"	No reflux
8	AI-35 Davison	10% H_2O	60	.10	Paraffinic	Rerun of run #6
9	AI-35 Davison	5% H_2O	60	.10	Paraffinic	Same conversion as 10% H_2O
10	AI-35 Davison	10% H_2O	420	.25	Paraffinic	Extended
11	AI-46 Houdry	10% H_2O	60	1.0	"Normal"	More active catalyst
12	AI-46 Houdry	None	5	.5	"Normal"	Indicates most cracking occurs early

*Relative to run #4

TABLE 2, Cont'd

RUN #	CATALYST	ADDITIVE	TIME Min.	CONVERSION %	DISTRIBUTION	COMMENTS
13	AI-46 #5	None	60	1.0	"Normal"	
14	AI-46 #5	10% H_2O	15	.25	"Normal"	Same conversion with and without water
15	AI-46 #5	10% H_2O	60	1.0	Normal"	
16	AI-35 Davison	10% H_2O	90	.10	Paraffinic	Attempted gas collection
17	CBZ-1 Davison	None	30	2.0	"Normal"	Most active catalyst contains zeolites
18	CBZ-1 Davison	10% H_2O	30	2.0	"Normal"	Cracking reaction delayed
19	AI-35 Davison	10% H_2O	45	.20	Paraffinic	High pressure in Parr autoclave
20	AI-35 Davison	None	60	1.0	"Normal"	Hexadecene reactant
21	AI-35 Davison	10% H_2O	60	.10	"Normal"	Hexadecene reactant

(which was confirmed in several repeat runs) the liquid products were much more evenly distributed through the C_4-C_{14} range with minimal chain branching and an unusually high paraffin/olefin ratio indicative of hydrogen transfer. Figure 1 shows the liquid product distribution over this catalyst in the absence of water (the same product distribution was obtained with the other three catalysts, both in the presence and absence of water) and the quite different product distribution obtained in the presence of water. This phenomena was also found to prevail in a run at more severe conditions (300°C and 2000 psi pressure for 45 min), carried out in an autoclave to obtain higher conversion. This latter run exhibited the expected increase in the amount of cracked product without a change in the product distribution previously encountered with this catalyst in the presence of water. Details of various runs are shown in Table 2.

It seems that a carbonium ion mechanism cannot explain the absence of olefins and branched chain hydrocarbons. The product distribution, except for the lack of olefins, more resembles a free-radical reaction. There is also no satisfactory explanation for the source of the hydrogen necessary to form saturated hydrocarbons from the parent hexadecane. Complicating the situation further is the lack of variables which can account for the different behavior of similar silica-alumina catalysts (35 and 46 activity). Variation of reaction time has demonstrated that neither product distribution changes during the course of the reaction, hence there is no sequential change in mechanism. There is a possibility, however, that although the total coke formation is greater in the absence of water, the amount of coke deposited proportional to the weight of cracked products may be higher with liquid water present. Formation of this coke could yield an adequate source of hydrogen, but this does not explain why this should occur only in the presence of the lower activity catalyst.

D) Conclusions

The premise that the presence of liquid water might increase catalytic cracking activity was found to be invalid. It was demonstrated that cracking can occur at previously unobserved low temperatures (though at low conversions) and that an anomoly exists in that one of the catalysts tested shows an entirely different cracking behavior and probably follows a different cracking mechanism.

The results of this work have been published in the Journal of Catalysis, 66, 463, (1980).

E) References

1. Thomas, C. L., "Chemistry of Catalytic Cracking," Ind.Eng. Chem., 41, 2565, (Nov. 1949)

2. Katzer, J. R., "Catalytic Cracking Chemistry" Notes from Catalysis course at Univ. of Delaware, Newark Del., 1975.

3. Haensel, V., "Catalytic Cracking of Pure Hydrocarbons," Advances in Catalysis III, Academic Press, NY, 1951

4. Hansford, R. C., "Chemical Concepts of Catalytic Cracking," Advances in Catalysis IV, Academic Press, NY, 1952

5. Emmett, P. H., "Oxidation, Hydration, Dehydration, and Cracking Catalysts," Catalysis, v. 7, Rheinhold Pub. Corp., NY, 1960.

6. Thomas, C. L., Catalytic Processes and Proven Catalysts, Academic Press, NY, 1970

7. Houdry, E. J., Burt, W.F., Peru, A. C., Peters, Petroleum Refiner 17, 574, (1938)

8. Murphree, E. V., Brown, C. L., Fischer, H. G. M., Gohr, E. J., Sweeney, W. J., "Fluid Cracking Process, Catalytic Cracking of Petroleum," Ind. Eng. Chem., 35, 768, (1943)

9. Simpson, T. P., Evans, L.P., Hornberg, C. V., and Payne, J. W., Proc. Am. Petroleum Inst. 24, 83 (1943)

10. Oblad, A. G., Milliken, T.H., Mills,G. A., "Chemical Characteristics of Cracking Catalysts," Advances in Catalysis III, Academic Press, NY, 1951.

11. Grensfelder, B. S., Voge, HH., Good, G. M., "Catalytic and Thermal Cracking of Pure Hydrocarbons," Ind. Eng. Chem., 4, 2573 (1949)

12. Hansford, R. C., Physical Chemistry of Hydrocarbons II, Academic Press, NY, 1952

Section II

Fischer-Tropsch Reactor Studies

A) Background

In 1925, Franz Fischer and Hans Tropsch discovered that reduced iron could be used to catalyze an atmospheric reaction of carbon monoxide and hydrogen to form hydrocarbons (1). Realizing that this reaction had important long-range possibilities for nations short in petroleum reserves, the development of the Fischer-Tropsch synthesis proceeded rapidly for a period of nearly twenty years. Commercial plants were constructed in Germany, Japan, and the United States, and were used chiefly for the production of gasoline and diesel fuel. A total of eight plants were erected in Germany for generating fuel for the military from 1935 to 1945. An extensive program was also carried out within the United States, eventually leading to the construction of a large pilot plant in Corpus Christy, Texas. In the early 1950's, however, the demand for gasoline decreased simultaneously with the development of foreign oil fields in the Middle East, Africa, and South America. Fischer-Tropsch reactions could not hope to compete economically with these new reserves, and research went through a dormant stage for nearly two decades (1,2). At the present time, only two commercial plants are in operation, both located in South Africa, and heavily subsidized by the government.

Although research on Fischer-Tropsch synthesis dates back more than fifty years, it has received renewed interest only since the end of an era of inexpensive foreign oil supplies. Coal, a tremendous potential energy resource in the United States, can be gasified to produce large quantities of carbon monoxide and hydrogen, which can in turn be transformed into liquid hydrocarbons by means of the Fischer-Tropsch synthesis. As this synthetic fuel process has approached economic competitiveness due to the rise in crude oil prices, it has become increasingly important to solve problems related to reactor scale-up. Since the Fischer-Tropsch reaction is a highly exothermic reaction, temperature control has been a key factor in the design of Fischer-Tropsch reactors. A design which allows excessive temperature rises within the reactor leads to premature catalyst deactivation and reactor plugging (2, 3, 4).

Detailed descriptions of the Fischer-Tropsch process and its modifications are available in the literature (1; 5-10). A number of raw materials are available for conversion, including coal, tar sands, and oil shale--each of which can be gasified in the presence of steam or oxygen. Lurgi gasifiers, as used by SASOL in South Africa, produce synthesis gas with a H_2/CO ratio greater than one,

which is then purified to remove sulfur and other catalyst poisons. Modern gasifiers produce lower (less than one) ratios of hydrogen to CO. In order to improve reactor life (by avoiding plugging), the H_2/CO ratio is then increased by means of the water-gas shift reaction:

$$CO + H_2O \longrightarrow CO_2 + H_2$$

This reaction also occurs in the synthesis reactor itself. Past experience (for example at SASOL) has shown that hydrogen to carbon monoxide ratios in excess of one and usually nearer two are required for sufficient reactor stability. External water-gas shift, however, creates a significant expense in the economics of the overall process, and there must be a trade-off between catalyst life and hydrogen production. It would be very desirable to eliminate the necessity of the water-gas shift reaction by improving the design of the synthesis reactor so that carbon monoxide and hydrogen could be used at H_2 to CO ratios of one or less without reactor malfunctioning.

Plugging becomes a problem at higher concentrations of carbon monoxide for two reasons. First, higher molecular weight products are favored, some of which remain as heavy waxes on the catalyst surface. Secondly, surface carbon from dissociated CO

$$CO \rightleftharpoons CO_s \longrightarrow C_s + O_s$$

(oxygen is removed from the surface in the form of CO_2 or water) is more likely to polymerize into graphitic carbon networks (11) forming an inert covering on the catalyst. This occurs since there is less hydrogen available to hydrogenate the surface carbon to initiate a chain growing sequence for hydrocarbon formation.

A proposed solution to this problem has been developed by Herbert Koelbel who began work in 1938 on a slurry bed Fischer-Tropsch reactor. With a slurry bed, the reactant gas is bubbled through a low volatility liquid medium containing a suspension of fine catalyst particles. Products are generally of sufficient volatility to pass through the reactor along with unreacted carbon monoxide and hydrogen. Further details of slurry bed operation and Koelbel's work are available in the literature (12-16).

Some of the process problems which can be improved by the slurry bed arrangement are summarized by Koelbel as follows (16):

a) Uniform temperature in the reactor and excellent heat exchange.

b) Reactant ratios of hydrogen to CO of as low as 0.6 can be utilized.

c) High contact and reactor efficiency

d) High conversion without recycle

However, there are also a number of disadvantages involved with the slurry bed system. With the catalyst suspended in the liquid, the reactant gases must first dissolve in the oil before they can contact the catalyst surface for reaction. Because of this, mass transfer limitations may arise. There is also a very low concentration of catalyst (relative to a fixed bed) which therefore requires a large reactor volume for comparable production levels. Additional problems may arise from product separation from the slurry oil, and handling (transport) of the slurry itself.

B) Work Hypothesis

The purpose of the study is to explain the difference between fixed bed and slurry-type Fischer-Tropsch reactors in regard to the higher tolerance for CO rich synthesis gas of the slurry reactor. This may be due to (1) the greater isothermicity of the slurry reactor; (2) mass transfer constraints at the gas-liquid interface of the slurry reactor.

The importance of isothermicity was investigated in fixed bed reactors of different diameter and therefore, different wall/volume ratios. The mass transfer phenomena were investigated in an experimental slurry reactor and by means of a computer model based on the reactor.

C) Work Performed and Discussion

1) Fixed Bed Reactors

The utilization of fixed bed reactors for Fischer-Tropsch synthesis, while commercially practiced (1; 2; 9) presents some inherent difficulties. Among them are: the need for rapid heat removal in a highly exothermic reaction, which has led to the installation of fluid bed reactors and of specifications for length/diameter ratios at various space velocities for fixed bed reactors (19); and the requirement for relatively high H_2/CO ratios (> 2:1) in the synthesis gas to prevent catalyst deactivation and reactor plugging. The advent of second and third generation gasifiers, all of which produce relatively low H_2/CO ratio synthesis gas (4) has emphasized the desirability to operate Fischer-Tropsch reactors with such low H_2/CO ratio gas without having to go through extensive and energy inefficient external water/gas shift steps. There has consequently been renewed interest in the slurry-type, three-phase Fischer-Tropsch reactor, first proposed by Kölbel (16;17; 18). Among the advantages claimed for the slurry reactor are: uniformity of reactor temperature; catalyst tolerance of H_2/CO feed ratios as low as 0.6; high conversion without external gas recycle. The disadvantages of slurry reactors are: the need for relatively large reactor volumes, because of low catalyst loadings; and the separation of high-boiling reaction

products from the liquid phase needed to suspend the catalyst.

In the present study, we have investigated the extent to which better reactor isothermicity and the suppression of reactor plugging can be achieved by reducing the diameter of a fixed bed reactor, containing an iron catalyst. Conclusions on the relationship between isothermicity and tolerance for low H_2/CO ratio synthesis gas in fixed bed reactors assist in the explanation of differences previously observed in the tolerance level for such gas between fixed bed and slurry bed reactors.

i) Equipment

Equipment was designed to permit operation at high conversion with single pass fixed bed reactors of different diameters. The reactors consisted of replaceable stainless steel tubes ranging from one quarter inch O.D. (U-tube, approximately 13" long) to 1" OD. (lengths of 5") with a wall thickness of .028." The reactors were heated by means of a Techne Sandbath (model SBL-2D) which provided a working volume 12" deep by 9" in diameter. Bath temperature was uniform to within $1/2^{o}C$ and varied by no more than $3^{o}C$ at $300^{o}C$ during the course of the reaction. The flow rate of the reactant mixture was monitored during the reaction using both a rotameter and a bubble flow meter and typically set at 20 to 150 cc per minute. Products consisted of carbon dioxide and hydrocarbons ranging from methane to components with molecular weights in excess of C_{30}. Liquid products in the effluent from the reactor were collected by means of an ice trap, and less condensable products were either vented or analyzed by gas chromatography. For short runs, a small volume trap was used to minimize lag time and to make it possible to follow the rapid initial deactivation during carbiding.

Gas samples could be taken at any time during a run by means of a Carle six port gas sampling valve, while liquid samples could only be analyzed as an integrated product at the conclusion of the run. A varian model 3760 gas chromatograph equipped with two columns was used to analyze product composition and determine over-all carbon monoxide conversion.

ii) Experimental Procedure

For all runs in this investigation, an equal amount of ammonia synthesis catalyst (United Catalyst Incorporated, Girdler Catalyst C73-1) was utilized. This catalyst is a low surface area (0.24 m^2/gm) unsupported iron catalyst, singly promoted with 0.8% potassium. Fresh catalyst was used in each run with the same catalyst pretreatment to insure a consistent starting point for each experiment. The catalyst was ground to between 30 and 60 mesh and reduced in flowing hydrogen at a GHSV of 1500 cc per gram per hour at $300^{o}C$ and 2 atmospheres for a period of 16 hours.

Following reduction, the reactor was purged with helium for approximately 0.5 hours prior to introduction of the reaction mixture. During this time, the reactor was adjusted to operating conditions in the general range of 275°C to 325°C and 132-150 psig pressure. Premixed cylinders of carbon monoxide and hydrogen were used in order to provide uniformity of the H_2/CO ratio in similar runs. After purging, the reaction mixture was charged and two process variables were observed: reactor plugging and catalyst deactivation. Gas samples were used to follow the deactivation of the catalyst by monitoring both the concentration of carbon monoxide in the exit gas as well as the exit gas flow rate. The onset of plugging could be observed directly be measuring the pressure differential across the reactor.

iii) Results

A major concern of this investigation was the effect of reactor diameter and reaction conditions on long-term deactivation of the catalyst. As the bed diameter increases, there is relatively less wall area per unit of catalyst volume for heat transfer from the reactor to the environment. Local instabilities can therefore occur, resulting in high surface temperatures on the catalyst or "hot spots." These hot spots may cause catalyst deactivation and reactor plugging.

Conditions chosen for operation with the different diameter reactors were intended to yield an over-all conversion of about 50% (temperature 300°C; pressure 10 atmospheres; GHSV equal to 80 cc per gram per hour and variable H_2/CO ratio) and the run was allowed to proceed for approximately 100 hours or until plugging was observed, whichever occurred first. Figure 2 shows runs for the two reactors of 1/4" and 1" diameter at a H_2/CO ratio of 1. Although there seems to be a minor difference in the rate of deactivation in the first half of the run, the plateau phase is the same in each case, and there is no plugging or sudden loss of activity for the remainder of either run. An internal thermocouple showed no temperature rise in the smaller reactor and a temperature rise of about 10°C in the 1" reactor. The initial loss of CO conversion shown in this figure is attributed to carbiding of the catalyst.

Runs in the smaller 1/4" reactor at different lower gas space velocities and lower H_2/CO ratios of 0.6 and 0.8 resp. (Fig. 3) demonstrate development of pressure drop after certain periods of time, such pressure drop occurring earlier at lower H_2/CO and lower space velocity. When the temperature was raised from 300 to 325° in the small diameter reactor pressure drop developed and increased rapidly already after about 40 hours on stream even at a H_2/CO ratio of 1 and relatively high space velocity (Fig. 4). The importance of temperature on plugging is evident.

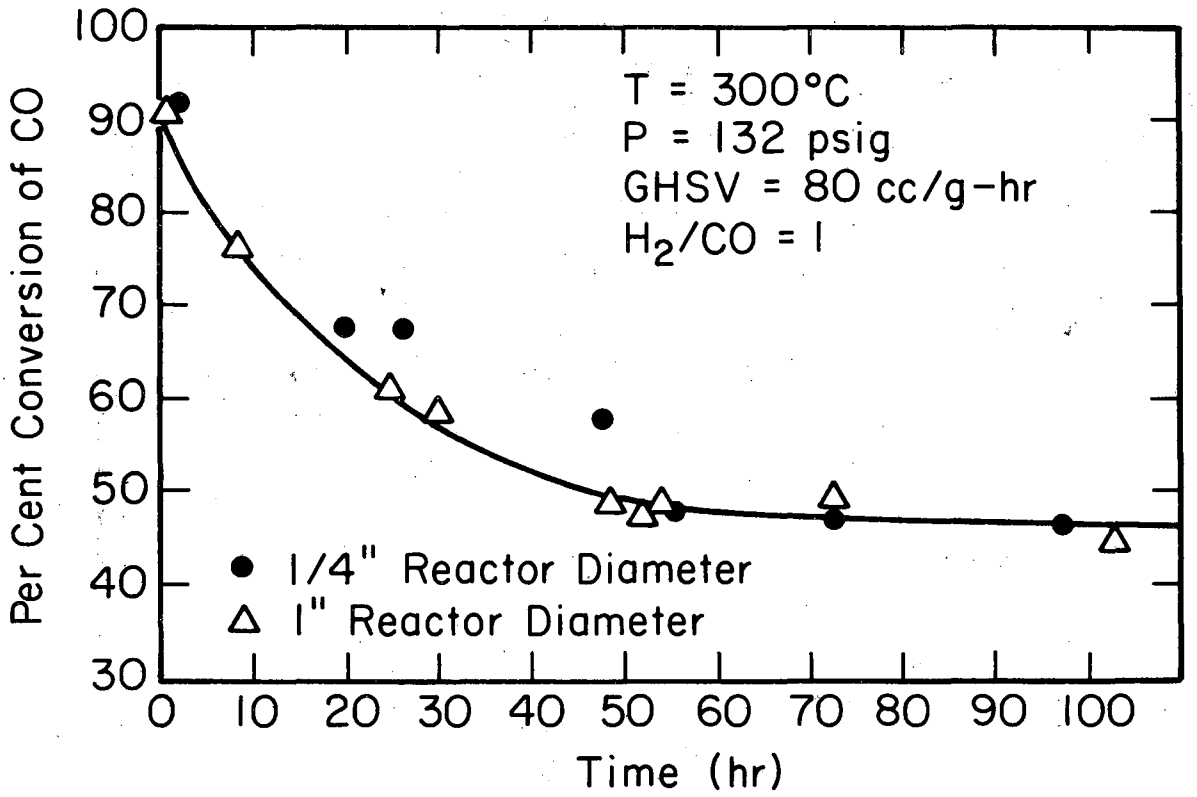

XBL 806-9911

Figure 2

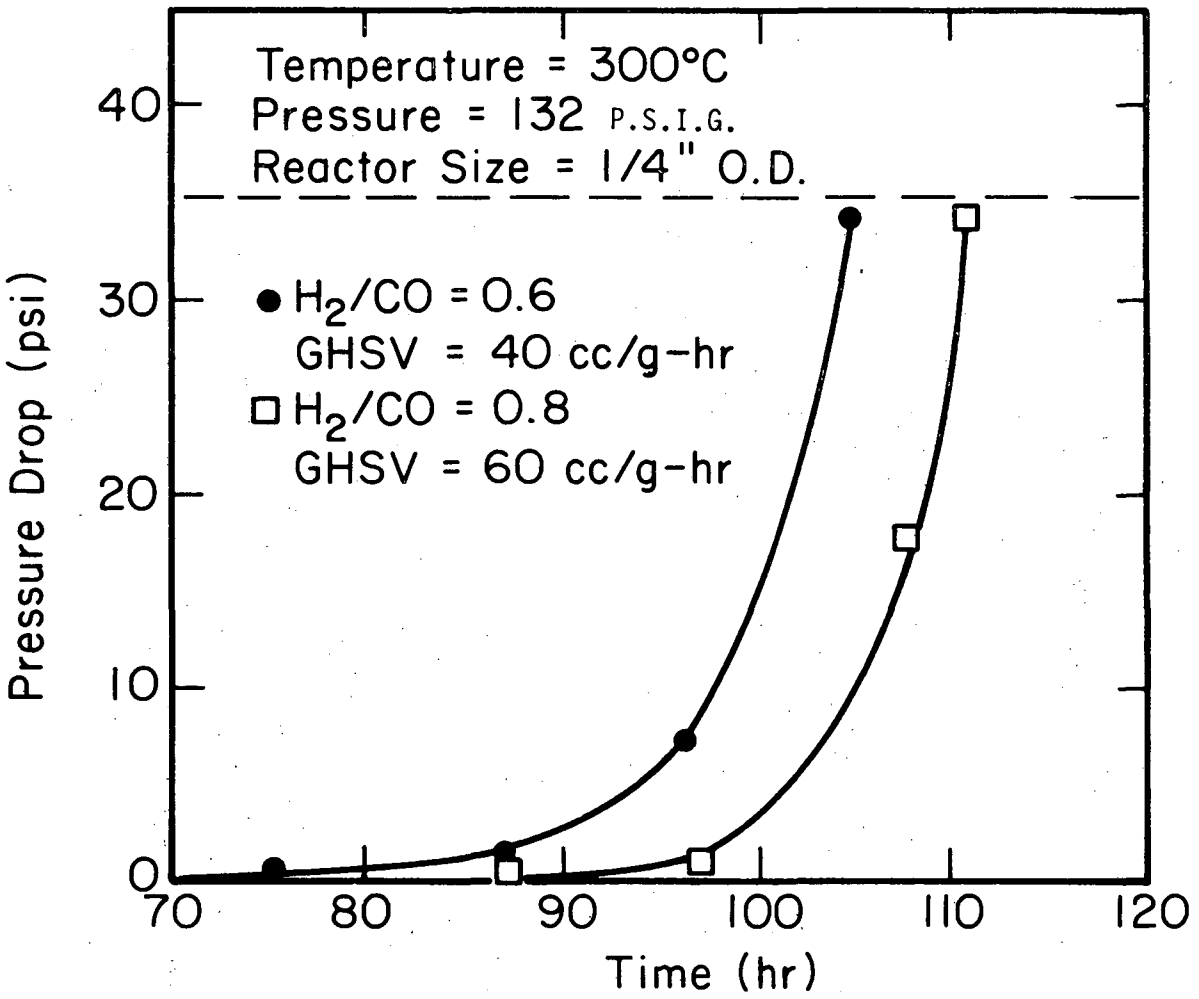

XBL 806-9905

Figure 3

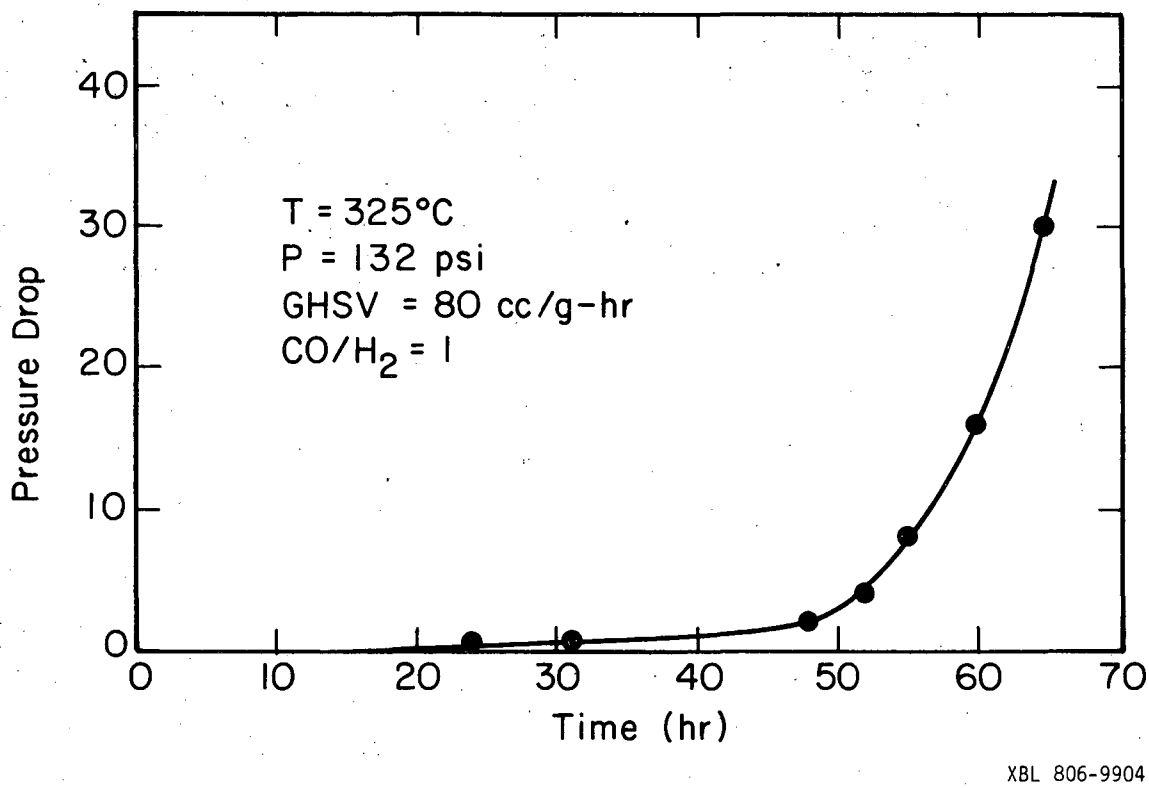
T = 325°C
P = 132 psi
GHSV = 80 cc/g-hr
CO/H2 = 1
Pressure Drop
Time (hr)
0
10
20
30
40
50
60
70
XBL 806-9904

Figure 4

Reduction of the H_2/CO ratio from 1 to 0.8 resulted in a pressure drop developing in both reactors but developing in the larger diameter reactor at a shorter time on stream than in the smaller diameter as shown in Figure 5.

An attempt was then made to determine the effect of temperature at a H_2/CO ratio of 1 for both reactors by determining the pressure drop after 90 hours on stream at different sand bath temperatures. This is shown in Figure 6. It is apparent that there is a critical temperature of about 275°C above which the 1" diameter reactor begins to show plugging after about 90 hours on stream at a hydrogen/CO ratio of 1 and a gas hourly space velocity of 80cc per gram per hour. The 1/4" reactor shows the plugging phenomena at a temperature about 20°C higher than that of the 1" reactor.

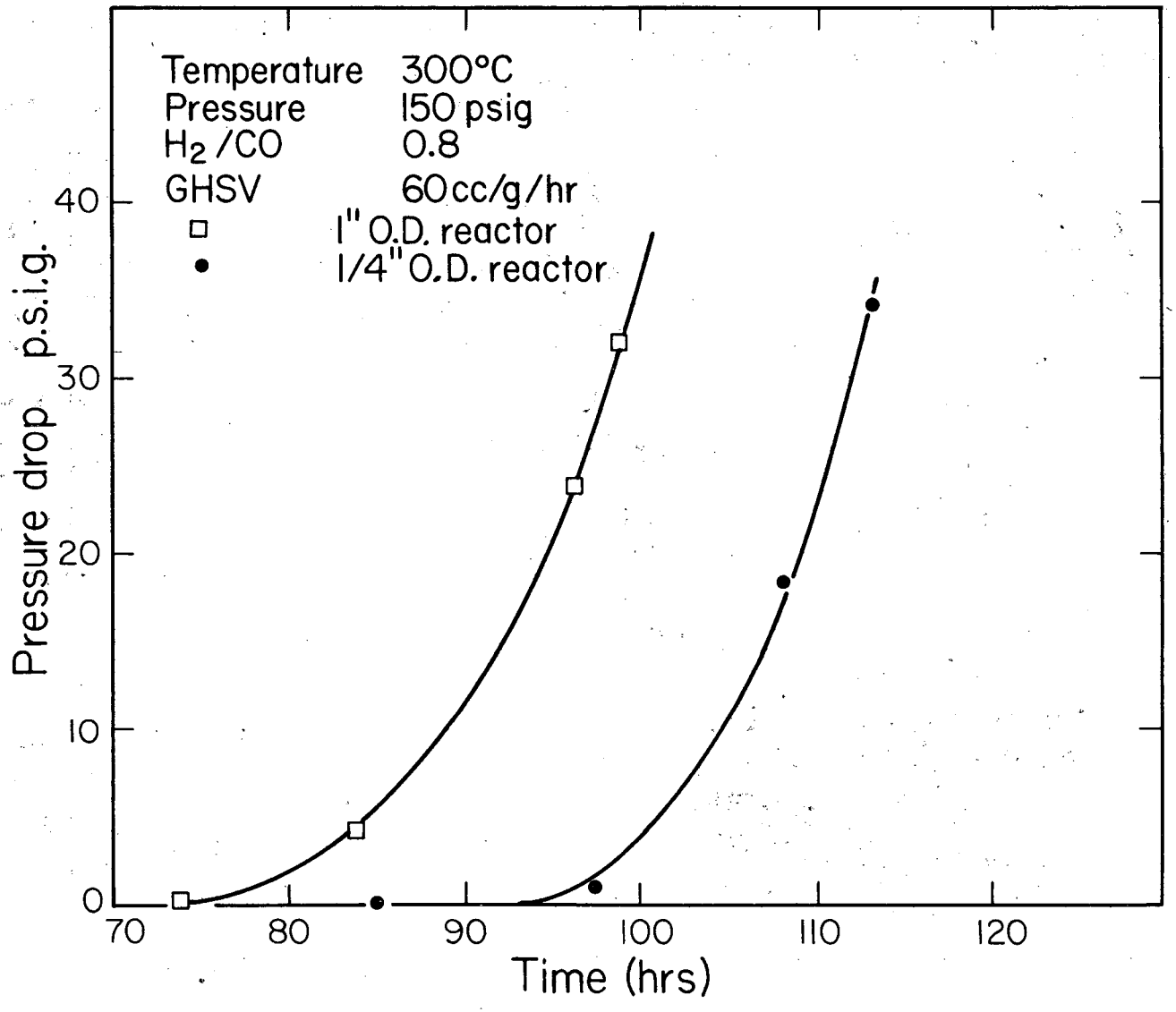

Figure 5

XBL 814-762

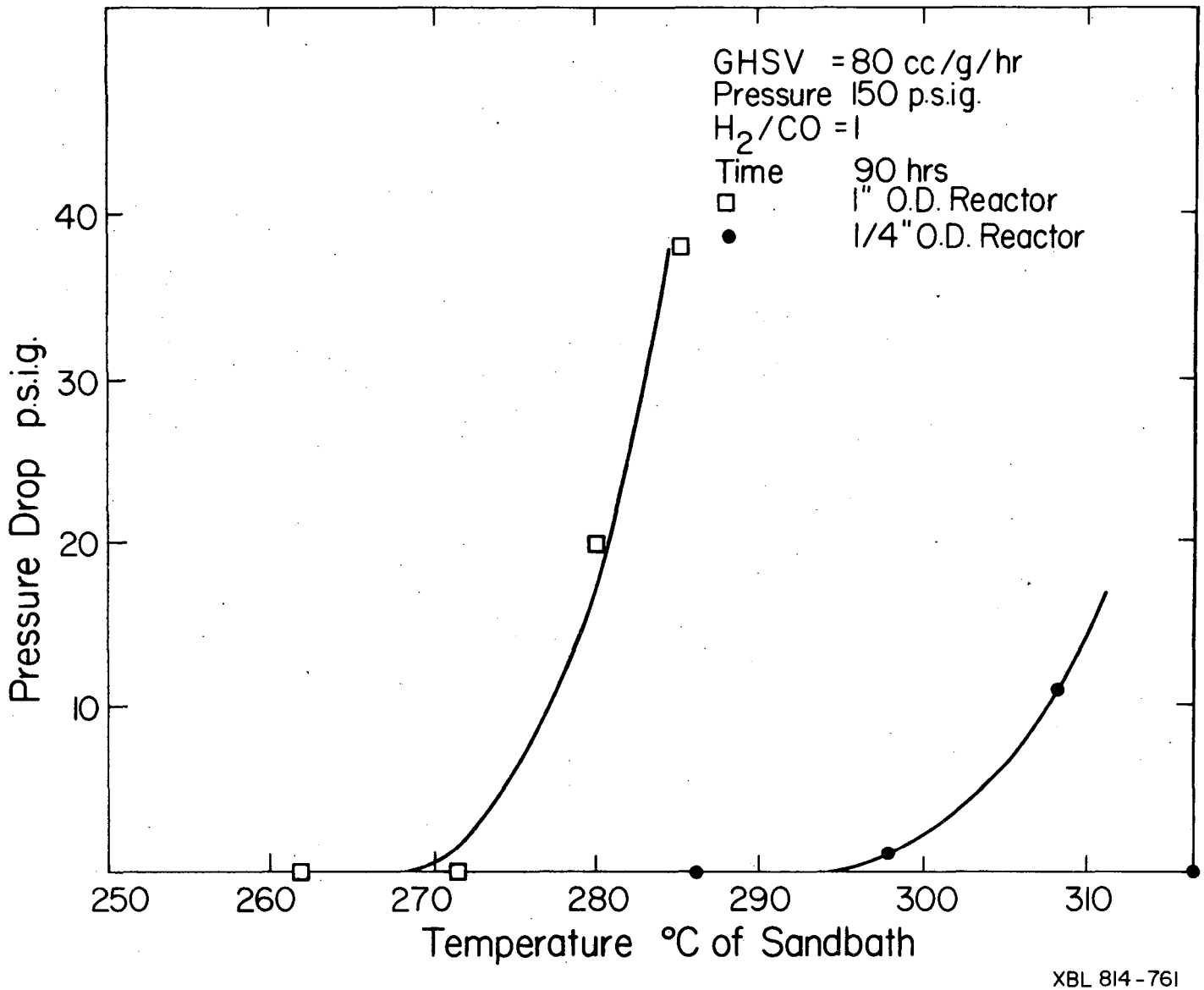
GHSV = 80 cc/g/hr
Pressure 150 p.s.ig.
$H_2/CO = 1$
Time 90 hrs
1" O.D. Reactor
1/4" O.D. Reactor
Pressure Drop p.s.i.g.
40
30
20
10
250
260
270
280
290
300
310
Temperature °C of Sandbath
XBL 814-761

Figure 6

iv) Conclusions

The findings of this study indicate that the diameter of a fixed-bed Fischer-Tropsch reactor critically affects the resistance of the reactor to plugging caused by the build up of carbonaceous or waxy deposits. At a fixed temperature and space velocity, plugging occurs at a shorter time on stream the larger the reactor diameter. Plugging is also accelerated by operation at high temperatures and low H_2/CO ratios. While the cause of plugging has not been established, it is very likely due to local nonuniformity in the catalyst temperature. Hot spots in the reactor are expected to occur since the heat release associated with Fischer-Tropsch synthesis is very high and the catalyst thermal conductivity is low. Decreasing the reactor diameter at a fixed gas space velocity, should improve temperature uniformity by decreasing the length of the thermal conduction path and increasing the extent of convective heat transfer from each catalyst particle. The latter effect can be ascribed to the higher gas velocity in a smaller diameter reactor. The suppression of plugging at higher H_2/CO ratios is likely due to a reduction in the product average molecular weight and the reaction with hydrogen of carbon deposited via the Boudouard reaction. A slurry bed reactor with its much greater isothermicity can be expected to behave similarly to very small diameter fixed bed reactors and therefore have a higher tolerance of lower H_2/CO ratio feed gas.

V. REFERENCES

1. Pichler, H., "Twenty-five Years of Synthesis of Gasoline by Catalytic Conversion of Carbon Monoxide And H_2," Advances in Catalysis, v. 4, Academic Press, NY, 1952

2. Dry, M. E., Shingles, T. J., Boshoff, L. J., and Van H. Botha, C. S., "Factors Influencing the Formation of Carbon on Iron Fisher-Tropsch Catalysts," Journal of Catalysis, 17, (1970)

3. Anderson, R. B., "Hydrocarbon Synthesis, Hydrogenation, and Cyclization," Catalysis IV, Rheinhold Pub., Baltimore, MD, 1956

4. Shinnar, R. and Kuo, J. C. W., DOE report FE-2766-13, Dist. Category UC-90D, (1978).

5. Bileon, P., Helle, J. N., Sachtler, W.M.H., "Incorporation of Surface Carbon into Hydrocarbons During Fischer-Tropsch Synthesis: Mechanistic Implication," Journal of Catalysis, 58, (1979)

6. Rabo, J. A., Risch, A. P., and Poutsma, J. L., "The Mechanism of Hydrocarbon Synthesis From CO and H_2 Over Group VIII Metal Catalysts," Journal of Catalysis, 53, (1978)

7. Vannice, M. A., "Catalytic Synthesis of Hydrocarbons From CO and H_2," Catalysis Reviews, 14(2), (1976)

8. Matsumoto, H., Bennett, C., "Methanation and Fischer-Tropsch Reactions Over Fused Iron Catalysts," Journal of Catalysis, 53, (1978)

9. Weitkamp, A. W., Seelig, H. S., Bouman, N. J., Cody, W. E., "Products of the Hydrogenation of Carbon Monoxide Over an Iron Catalyst," Ind. Eng. Chem., 45, (Feb. 1953)

10. Joyner, R. W., "Mechanism of Hydrocarbon Synthesis from Carbon Monoxide and Hydrogen," Journal of Catalysis, 50, (1977)

11. Bonzel, H. P., Krebs, H. J., "On the Chemical Nature of the Carbonaceous Deposits on Iron After CO hydrogenation," Surface Science, 91, (1980)

12. Schleysinger, M. D., Orwell, J. H., Leva, M., Storch, H. H., "Fischer-Tropsch Synthesis in the Slurry Phase," Ind. Eng. Chem., 43, (June 1951)

13. Calderbank, P. H., Evans, Farley, Jepson, Poll, "Rate Processes in the Catalyst-Slurry Fischer-Tropsch Reaction," Catalysis in Practice, London, 1963

14. Koelbel, H., Ralek, M., "The Fischer-Tropsch Synthesis in the Liquid Phase," Report from the Chemical Eng. Institute, Technical University, Berlin, Germany.

15. Sherwood, T.K., Farkas, E.J., "Studies of the Slurry Reactor," Chemical Engineering Science, 21, (1966)

16. Kölbel, H. and Ralek, M., Catal. Rev. - Sci. Eng. 21 (2) 225 (1980)

17. Kolbel H., Ackerman, P., and Engelhardt, F., Erdoel und Kohle 9, 153, 225, 303 (1956)

18. Kölbel, H., and Ackerman, P. Chem. - Ing. - Tech. 28, 381 (1956)

19. Chemierohstoffe aus Kohle," ed. J. Falbe, Georg Thieme Verlag, Stuttgart, 1977, p. 237-239.

2) Slurry Reactor

i) Introduction

Slurry or bubble column reactors offer a number of advantages over fixed and fluidized bed reactors for carrying out Fischer-Tropsch synthesis of hydrocarbons (7). These advantages include: (1) uniformity of catalyst temperature, due to slurry-phase backmixing; (2) capacity for operation at high syn-gas conversions, due to efficient heat transfer; (3) high selectivity to C_{5+} products, owing to the elimination of catalyst hot spots; (4) ability to use CO rich synthesis gas without reactor plugging or fouling of catalyst particles due to formation of carbonaceous deposits.

Examinations of the effects of mass transfer on Fischer-Tropsch synthesis in slurry reactors have been reported by Calderbank et al. (6), Zaidi et al. (7), Satterfield and Huff (8), and Deckwer et al. (9). All of these authors agree that the principal resistance to mass transfer occurs at the interface between the gas bubbles and the slurry; however, the extent to which the performance of a slurry reactor is limited by gas-liquid mass transfer has been the subject of some discussion. On the basis of an analysis of four experimental studies, Satterfield and Huff (8) conclude that H_2 mass transfer could definitely limit reactor productivity. Deckwer et al. (9) disagree with this conclusion and show, on the basis of their own analysis, that the mass-transfer resistance is small compared to the reaction resistance for all of the cases they examined. In a subsequent exchange of notes (10,11), it was established that the conclusions regarding the significance of mass transfer depend heavily on the bubble size used in the calculation of interfacial area. Satterfield and Huff (11) argue for a bubble size of 0.23 to 0.24 cm, while Deckwer et al. (11) contend that the bubbles have a diameter of only 0.07 cm. Since smaller bubbles result in a higher interfacial area and, hence, a lower resistance to mass transfer, the essence of the disagreement becomes apparent. It is also significant to note that in the earlier work of Calderbank et al. (6) it was observed that the release into the slurry of free carbon, formed via the Boudouard reaction, causes the slurry viscosity to increase which, in turn, brings about a decrease in the gas hold-up. This effect results in a progressive deterioration of the mass-transfer efficiency for H_2.

In the previous studies of mass-transfer effects, attention has centered exclusively on the significance of the H_2 mass-transfer resistance relative to the total reaction resistance. This focus was dictated by the fact that over iron, the most commonly used catalyst for Fischer-Tropsch synthesis, the kinetics for reactant consumption are first order in H_2

concentration. No effort was made in these studies to examine the influence of mass transfer on the concentration of CO in the liquid-phase. The neglect of this effect is significant, since one expects the mass-transfer coefficient for H_2 to be greater than that for CO and, hence, situations might occur in which the gradient for H_2 transfer through the liquid is less than that for CO. Under such circumstances, the H_2/CO ratio at the liquid-catalyst surface would be greater than that in the gas phase. Since the H_2/CO ratio at the catalyst surface affects the average molecular weight of the product and its olefin to parafin ratio, as well as the formation of free carbon, it becomes quite important to establish the extent to which gas-liquid mass transfer influences the H_2/CO ratio in the slurry. It was for this purpose that the present investigation was under-taken.

ii) Work Performed and Nomenclature

The work performed in this phase of the project was on two levels: experimental and computational. The nomenclature used in the following sections of this work is:

Q_G	gas volumetric flow rate, cm^3/sec
Q_L	liquid volumetric flow rate, cm^3/sec
V_R	volume of the reactor, cm^3
w	Catalyst loading, $\frac{\text{g catalyst}}{\text{liquid volume}}$, g/cm^3
z	vertical distance in the reactor, cm
a	gas-liquid interfacial area per unit volume, cm^{-1}
$C_{G,i}$	gas-phase concentration of component i, $moles/cm^3$
$C_{L,i}$	liquid-phase concentration of component i, $moles/cm^3$
$C^*_{L,i}$	liquid-phase concentration of component i that would be inequilibrium with C_{ig}, $moles/cm^3$
C_i^{max}	concentration when no mass transfer limitations exist, $moles/cm^3$
C_G	Total gas-phase concentration, $moles/cm^3$
k_o	rate constant for consumption of hydrogen, $\frac{\text{moles } H_2}{\text{sec-g catalyst}}$

$k_{L,i}$ mass transfer coefficient for the transfer of component i from the gas-liquid interface to the bulk liquid, cm/sec

L height of the reactor, cm

m_i solubility coefficient of component i, $\frac{\left(\frac{\text{moles}}{\text{cm}^3}\right)_G}{\left(\frac{\text{moles}}{\text{cm}^3}\right)_L}$

N_i Stanton number, $\frac{k_{L,i}aL}{M_i U_G^o}$ dimensionless

r_i rate of consumption of component i, $\frac{\text{moles}}{\text{sec-g catalyst}}$

Greek Symbols

$\theta_{G,i}$ dimensionless concentration, $C_{G,i}/C^o_{G,H_2}$

$\theta_{L,i}$ dimensionless concentration, $\frac{C_{L,i}m_i}{C^o_{G,H_2}}$

υ dimensionless gas-phase velocity, $\frac{U_G}{U_G^o}$

ν_i stoichiometric coefficient

ζ dimensionless distance, z/L

ϵ_G gas hold-up, $\frac{\text{volume of gas}}{\text{total volume}}$

τ_L liquid space time, V_R/Q_L

τ_G gas space time, L/U_G^o

a) Experimental Work

A slurry reactor has been built as shown in Fig. 7. It consisted of a 1.08 in. I.D. stainless steel tubing pipe, 6 ft long with sample ports every 12 in. The column was heated by resistance wiring and filled to about 2/3 height with a C_{20}-C_{30} wax. Metered gases were bubbled through the column entering through a 25-50 nm sintered bronze disk. Operation was at 10 atm pressure, temperatures of 270-320°C and H_2/CO ratios of 0.4 to 3.

The experiments have been aimed at measuring mass transfer coefficients and reaction kinetics, to be used in a model of the slurry reactor. The catalyst tends to cake, and sometimes plug the reactor. Experiments with a glass column, the geometry of which is similar to that of the pressure slurry reactor have led to the design of baffles that break up clumps of catalysts.

Data taken allow us to draw some conclusions about the Fischer-Tropsch slurry system. The rates of production of CO_2 and hydrocarbons through C_{10} were measured as a function of temperature and H_2/CO ratio (Tables 2 and 3). The catalyst was subjected to six days of reduction under 10 atm of hydrogen at a space velocity of 80 cm^3/min-g catalyst. The catalyst loading was 0.125g of catalyst/g slurry liquid. The data discussed here were taken over a 10-day period. Table 1 shows a schedule of the run after the first 50 hr, no deactivation was observed. The data shown were all taken during steady state operation. Table 2 shows rates of production of CO_2 and hydrocarbons through C_{10} as a function of temperature, at H_2/CO = 0.96 and P = 10 atm. If no water is produced, the rate at which carbon is incorporated into hydrocarbons will be equal to the rate of CO_2 production. The total rate of carbon incorporation through C_{10} is shown in the last column in Table 2. If this rate is lower than the rate of CO_2 production, some of the CO is consumed to make other products. The fate of this CO is not known. It may form surface carbon; it may react with the iron to make iron carbide; it may react with the slurry liquid; or it could make alcohols, which were present in small amounts. The formation of free carbon as observed by Calderbank (6) is also possible. If the rate of carbon incorporation into hydrocarbons is greater than the rate of CO_2 production, hydrogen must react on the catalyst surface to produce water. From the numbers in Table 2, it can be seen that at low temperature, water is produced. This is consistent with the equilibrium behavior of the water gas shift reaction: low temperature favors the production of water (1). As temperature increases, the rate of consumption of CO for other products

FIGURE 7

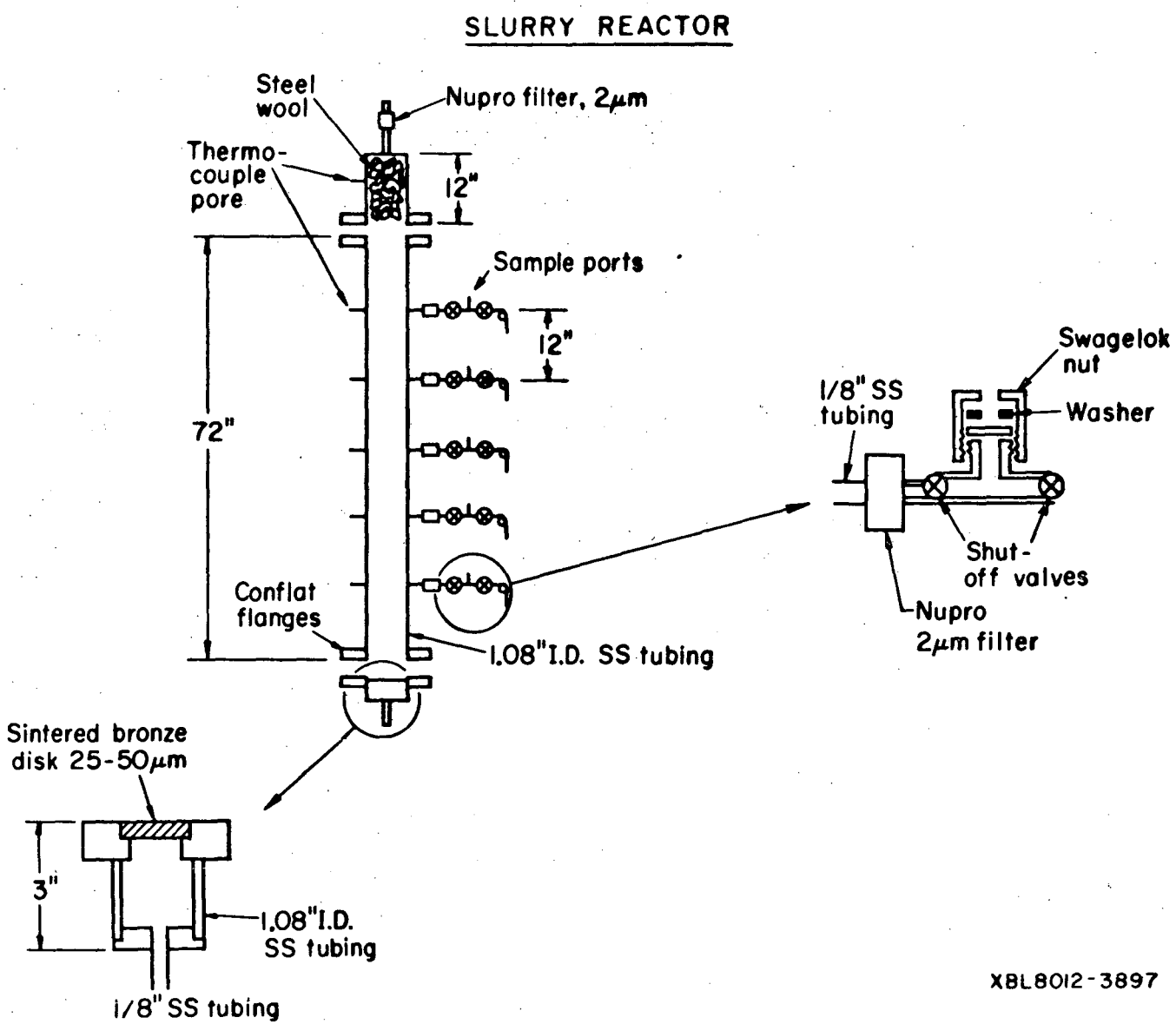
SLURRY REACTOR
Steel wool
Nupro filter, 2μm
Thermo-couple pore
12"
Sample ports
12"
72"
Swagelok nut
1/8" SS tubing
Washer
Shut-off valves
Nupro 2μm filter
Conflat flanges
1.08"I.D. SS tubing
Sintered bronze disk 25-50μm
3"
1.08"I.D. SS tubing
1/8" SS tubing
XBL8012-3897

Table 1

Schedule of the Run Reported Here

Time, Hours	Conditions
0-57	$H_2/CO = 1.0$
	$T = 300^oC$
57-76	$H_2/CO = 1.0$
	$T = 270^oC$
76-95	$H_2/CO = 1.0$
	$T = 285^oC$
95-100	$H_2/CO = 1.0$
	$T = 320^oC$
100-121	$H_2/CO = 1.0$
	$T = 300^oC$
121-165	$H_2/CO = 3.0$
	$T = 300^oC$
165-200	$H_2/CO = 2.0$
	$T = 300^oC$
200-213	$H_2/CO = .88$
	$T = 300^oC$
213-235	$H_2/CO = .374$
	$T = 300^oC$
235-240	$H_2/CO = 1.0$
	$T = 300^oC$

TABLE 2

$H_2/CO = .96$

Rates in moles/min-g catalyst

T	R_{CO_2} x10^4	R_{CH_4} x10^5	$R_{C_2^=}$ x10^5	R_{C_2} x10^6	$R_{C_3^=}$ x10^6	R_{C_3} x10^7	$R_{C_4^=}$ x10^6	R_{C_4} x10^7	$R_{C_5^=}$ x10^6	R_{C_5} x10^7	$R_{C_6^=}$ x10^6	R_{C_6} x10^6	$R_{C_7^=}$ x10^6	R_{C_7} x10^7	$R_{C_8^=}$ x10^6	R_{C_8} x10^7	$R_{C_9^=}$ x10^6	R_{C_9} x10^7	$R_{C_{10}^=}$ x10^6	$R_{C_{10}}$ x10^7	ΣnR_n x10^4
270°C	.144	.297	.106	.179	.67	2.15	.51	.787	.357	1.006	.286*		.153	.433	.203	.443	.175	.390	.131	.318	.213
285°C	.462	.657	.229	.343	-	-	1.275	1.41	.790	1.82	.597*		.427	.827	.427	.820	.399	.907	.302	.663	-
300°C	.833	1.32	.343	.770	2.53	3.53	2.20	3.09	1.45	2.84	.867*		.774	1.31	.674	1.17	.568	1.12	.414	.812	.780
320°C	1.70	2.38	.577	1.17	4.53	5.23	2.98	4.06	2.18	3.95	1.15*		1.49	3.07	1.40	2.54	1.12	2.09	.667	1.16	1.28

*$(R_6 + R_6^=) \times 10^6$

$R^=$ Denotes Rates of Olefin Formation
R Denotes Rates of Paraffin Formation

TABLE 3

T = 300°C; Rates in Moles/Min. g Catalyst

H_2/CO	R_{CO_2}	R_{CH_4}	$R_{C_2}^=$	R_{C_2}	$R_{C_3}^=$	R_{C_3}	$R_{C_4}^=$	R_{C_4}	$R_{C_5}^=$	R_{C_5}	$R_{C_6}^=$	R_{C_6}	$R_{C_7}^=$	R_{C_7}	$R_{C_8}^=$	R_{C_8}	$R_{C_9}^=$	R_{C_9}	$R_{C_{10}}^=$	$R_{C_{10}}$	ΣnR_n
	$\times 10^4$	$\times 10^5$	$\times 10^5$	$\times 10^6$	$\times 10^6$	$\times 10^6$	$\times 10^6$	$\times 10^6$	$\times 10^6$	$\times 10^7$	$\times 10^6$	$\times 10^7$	$\times 10^7$	$\times 10^7$	$\times 10^7$	$\times 10^7$	$\times 10^7$	$\times 10^8$	$\times 10^8$	$\times 10^8$	$\times 10^4$
2.953	2.410	3.54	1.00	2.61	9.2	1.45	4.9	1.00	2.75	6.8	1.43	3.38	9.60	2.27	5.57	1.30	2.90	7.43	8.33	1.88	1.62
2.00	2.79	2.84	1.04	2.31	9.17	1.64	4.87	.795	2.94	8.37	1.64	4.38	12.3	2.41	8.03	1.69	5.67	12.90	12.02	2.32	1.66
.881	1.54	1.31	.507	.84	3.60	.577	2.73	.399	2.02	4.33	*1.55		9.10	1.57	6.57	1.10	3.99	7.90	15.7	2.79	.913
.374	.697	.597	.259	.246	1.73	.105	1.44	.125	.930	2.43	*.524		4.10	.620	2.72	.457	1.70	2.79	3.42	.426	.403

*$(R_C + R_6^=)$

increases. This is consistent with McKee's (2) data on fixed bed reactors, which showed that carbon formation increased with temperature.

In Fig. 8, activation energy plots are shown for CO_2, CH_4, and C_2H_4. All of the curves show activation energies that decrease as temperature increases, although they remain relatively high. (31 K cal for CO_2.) This is an indication that mass transfer is starting to affect the rate of reaction. The mass transfer resistance appears to be at the gas-liquid interface: Calculations based on published correlations for k_La (3) and the measured rate of reaction at 300°C predict a slight concentration difference between the gas-liquid interface and the catalyst surface. Further, calculations based on the measured rate, using the correlation presented by Satterfield (4), show that under the conditions used, the reaction is far from an internal diffusion limited regime.

Figure 9 shows the product distribution as a function of temperature. The changes in product distribution, while not large, are consistent with other work in fixed beds. C_n/C_1 for a given n, decreases as temperature increases; light products are favored at high temperature.

Rates of reaction as a function of H_2/CO ratio are shown in Table 3. Again, the total rate of carbon consumption is shown. In every case, a significant amount of CO is reacting to produce something other than C_1 through C_{10} hydrocarbons. The fraction f of CO that goes to other products is given by

$$f = 1 - \frac{\Sigma\, nRcn}{R_{CO_2}}$$

f is not a strong function of H_2/CO; however, as we might expect, f increases as the H_2/CO ratio decreases.

The product distribution as a function of H_2/CO ratio is also shown in Fig. 10. As the H_2/CO ratio increases, the curve C_n/C_1 vs n becomes steeper; lighter products are favored.

Note that the rates of reaction at 300°C and H_2/CO = 0.88 are significantly different from those at H_2/CO = 0.96 and 300°C. This is believed to result from a higher degree of carbidization at H_2/CO = 0.96.

In conclusion, the catalyst does not deactivate significantly even at low H_2/CO ratios. Significant quantities of carbon are converted to products other than C_1-C_{10} hydrocarbons. In view of the fact that the

ACTIVATION ENERGY PLOT

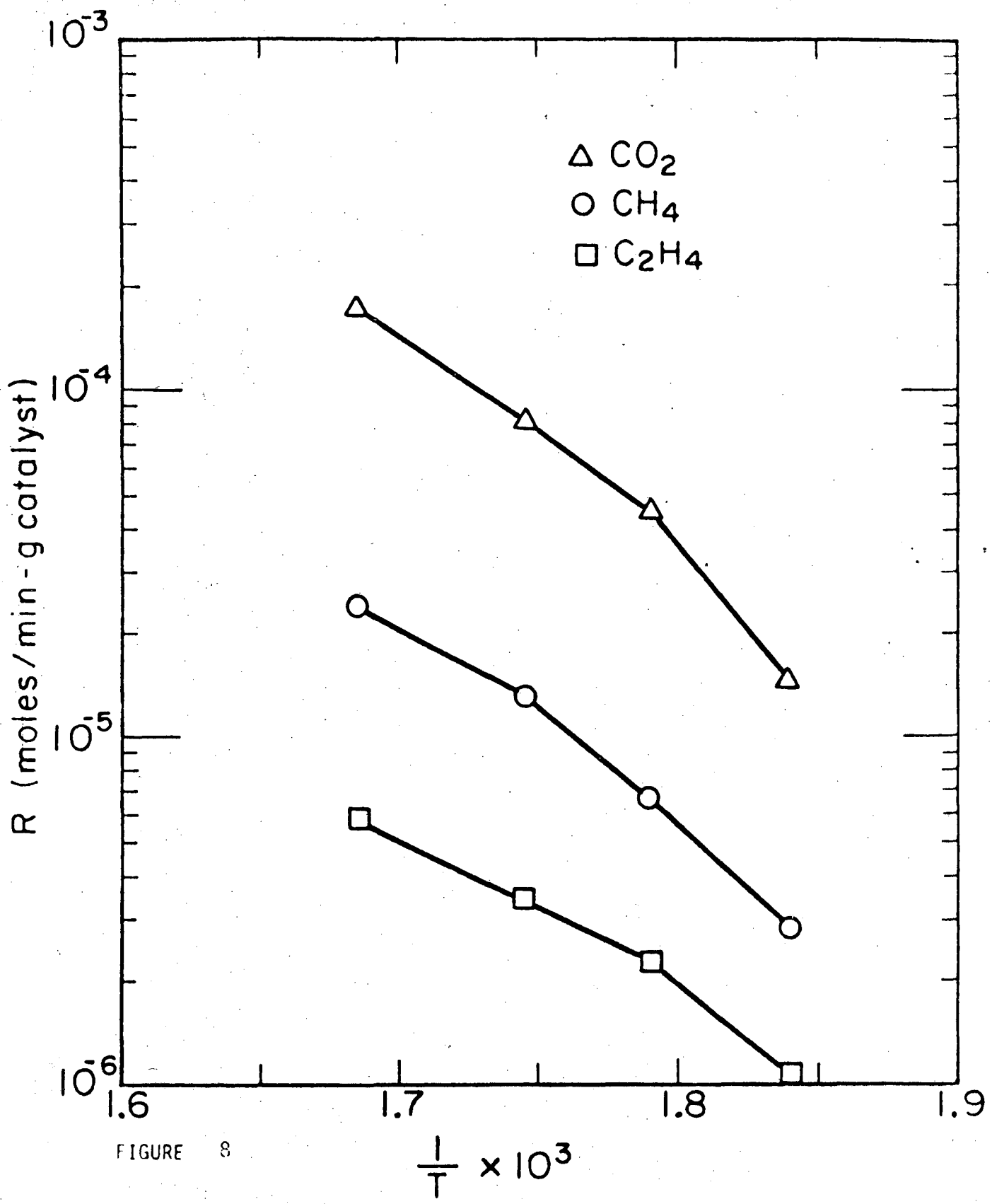

FIGURE 8

XBL814-3769

EFFECT OF TEMPERATURE ON PRODUCT DISTRIBUTION

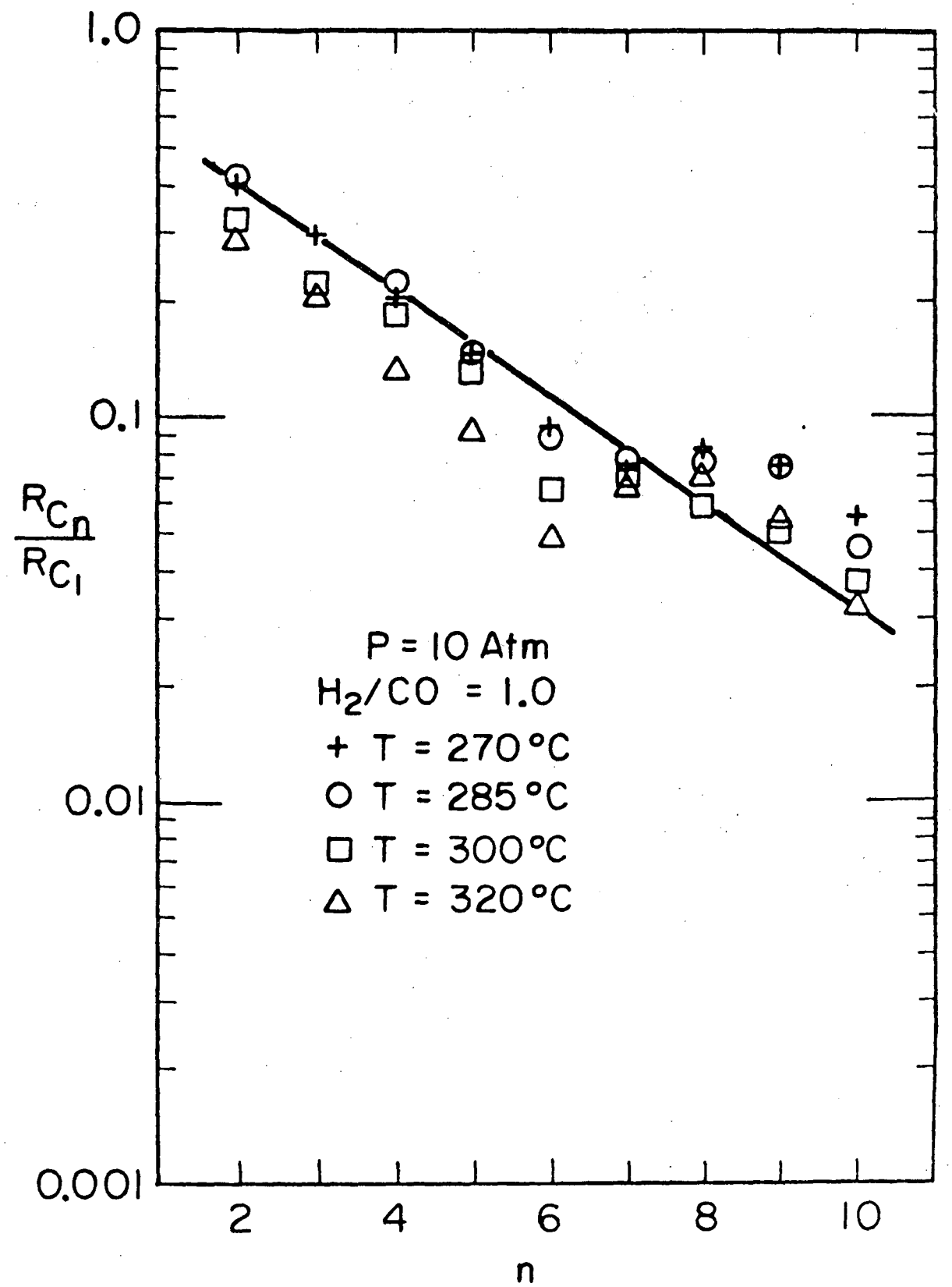

FIGURE. 9

XBL 814-3770

EFFECT OF H_2/CO RATIO ON PRODUCT DISTRIBUTION

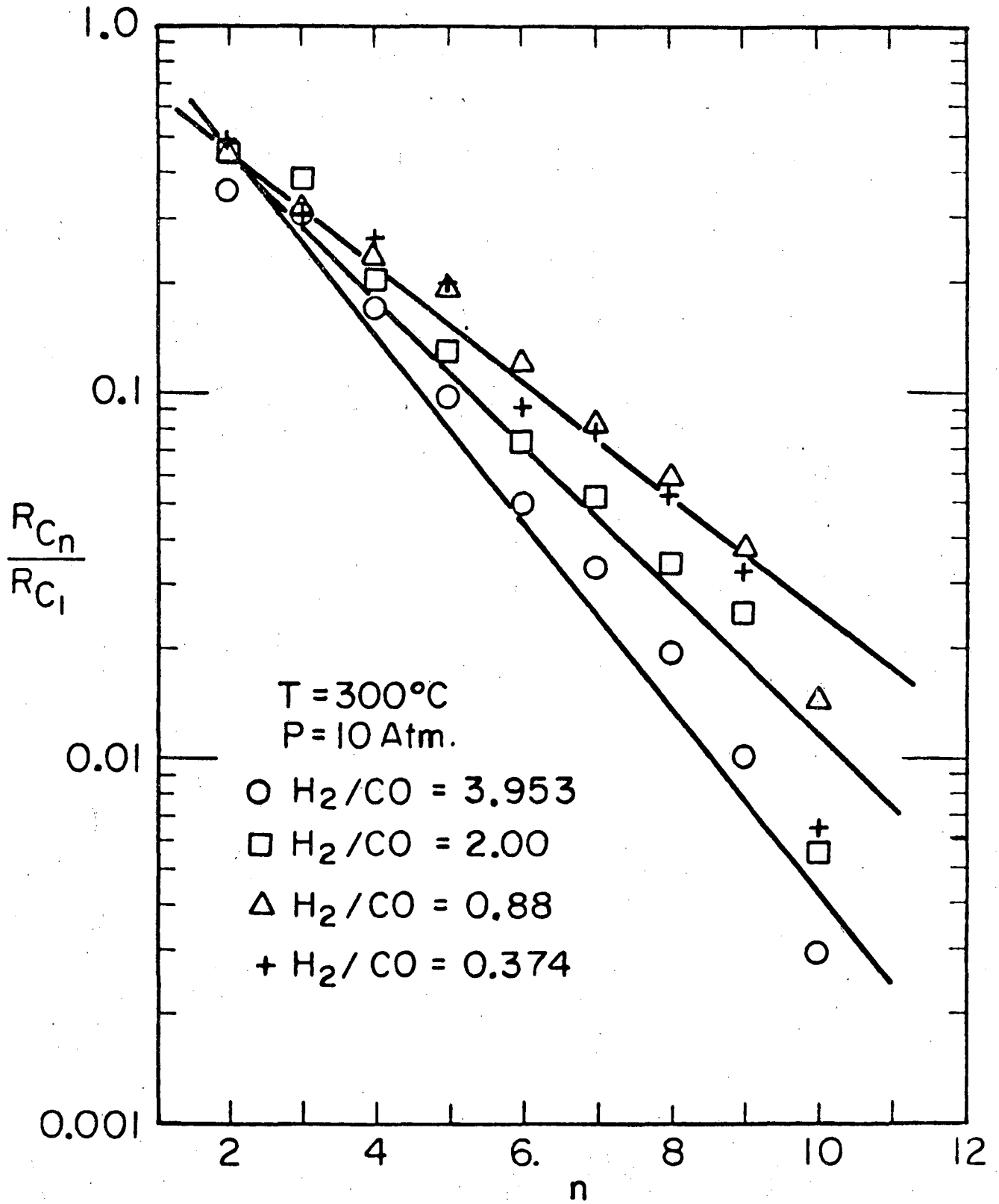

FIGURE 10

XBL814-3767

catalyst does not deactivate, it seems unlikely that surface carbon is being produced. Rather significant amounts of free carbon may be generated.

b) Reactor Model

The following assumptions were introduced to simplify the reactor model: (1) the liquid phase is well-mixed; (2) the catalyst is uniformly dispersed; (3) the gas is in plug flow; (4) the primary resistance to mass transfer is at the gas-liquid interface. It was further assumed that there is a small, but constant, flow of liquid into and out of the column.

The gas-phase mass balance for each component, written over a differential element of the reactor, is given by

$$-\frac{d(u_G C_{Gi})}{dz} = k_{L,i}a(C^*_{L,i} - C_{L,i}) \qquad (1)$$

where $C^*_{L,i} = C_{G,i}/m_i$. To account for changes in gas velocity with position in the column, one must also consider an overall mass balance, given by

$$-C_G \frac{du_G}{dz} = \sum_{i=1}^{n} k_{L,i}a(C^*_{L,i} - C_{L,i}) \qquad (2)$$

The boundary conditions on Eqs. 1 and 2, defined at $z = 0$, are

$$u_G = u^o_G$$

$$C_{G,i} = C^o_{G,i} \qquad (3)$$

The liquid-phase mass balance for each component, assuming that no reactant or product enters with the liquid, can be written as

$$-Q_L C_{L,i} + \int_0^{V_R} k_{L,i}a(C^*_{L,i} - C_{L,i})\, dV_r = V_r w(1 - \varepsilon_G)\, r_i \qquad (4)$$

If the average gas phase concentration for each component is defined as

$$\overline{C}_{G,i} = \frac{1}{V_r} \int_0^{V_R} C_{G,i} dV_r \quad , \qquad (5)$$

then Eq. 4 can be written as

$$-Q_L C_{1,i} + V_r k_{L,i} a(\bar{C}^*_{L,i} - C_{L,i}) = V_r w(1 - \varepsilon_G)\, r_i \qquad (6)$$

Equations 1, 2, 5 and 6 are non-dimensionalized by use of the following definitions

$$\theta_{G,i} = C_{G,i}/C^o_{G,H_2} \qquad v = u_G/u^o_G$$

$$\theta_{L,i} = C_{L,i} m_i/C^o_{G,H_2} \qquad \tau_G = L/u^o_G \qquad (7)$$

$$\tau_L = V_r/Q_L$$

$$\theta_G = C_G/C^o_{G,H_2} \qquad N_i = \frac{k_{L,i} a\, L}{m_i u^o_G}$$

Thus,

$$-\frac{d(v\,\theta_{G,i})}{d\zeta} = N_i(\theta_{G,i} - \theta_{L,i}) \qquad (8)$$

$$-\theta G \frac{dv}{d\zeta} = \sum_{i=1}^{n} N_i \theta_{G,i}\, d\zeta \qquad (9)$$

$$-\theta_{G,i} = \int_0^1 \theta_{G,i}\, d\zeta \qquad (10)$$

$$-\theta_{L,i} + N_i \frac{m_i \tau_L}{\tau_G}(\bar{\theta}_{G,i} - \theta_{L,i}) = \frac{m_i V_r w(1 - \varepsilon_G)\, r_i}{Q_L C^o_{G,H_2}} \qquad (11)$$

The dimensionless group N_i appearing in Eqs. 8, 9, 11 is the Stanton number for component i and represents the ratio of the gas space time to the characteristic time for liquid-phase mass transfer.

Studies by several groups (12,13) have shown that the kinetics of methane synthesis and CO consumption over iron catalysts are, to a good approximation, first order in H_2 concentration and zero order in CO concentration. Accordingly, the rate of formation or consumption of component i can be represented by

$$r_i = \nu_i k_o C_{4}, H_2 \qquad (12)$$

Substitution of Eq. 12 into Eq. 11, allows us to rewrite Eq. 11 as

$$-\theta_{L,i} + N_i \frac{\tau_L}{\tau_G} (\bar{\theta}_{G,i} - \theta_{L,i}) = \nu_i Da \frac{\tau_L}{\tau_G} \frac{m_i}{mH_2} \theta_{L,H_2} \qquad (13)$$

The dimensionless group Da appearing in Eq. 13 is the Damkohler number, which is defined as

$$Da = \frac{Lw(1 - \varepsilon_G) k_o}{u_G^o} \qquad (14)$$

α) Parameter Estimation

Values for the solubility coefficients and their sources are listed in Table 4. Solubilities for H_2, CO, CO_2, and H_2O in wax of molecular weight 350 were measured at temperatures up to 300°C by Peter and Weinert (22). The solubility parameter for CH_4 in wax was estimated from the solubility of CH_4 in dodecane at 25°C using Raoult's law. The solubility of C_5H_{10} was estimated from data on CH_4, C_2H_6, and C_3H_8 at 25°C by extrapolating to higher temperature using Raoult's law, and further extrapolating to higher carbon number.

An interfacial area of 4 cm^{-1} was used for most of the computations reported here. This value corresponds to the plateau in the curve of interfacial area vs. superficial gas velocity observed for velocities in excess of 4 cm/s by Calderbank et al. (6). Zaidi et al. (7) have made similar measurements but report interfacial areas roughly a factor of two greater than those measured by Calderbank et al. (6). The reason for the higher values of a reported by Zaidi et al. (7) is most likely due to the fact that they used a sintered plate gas distributor rather than a sparger to introduce the gas into the column. Since it is more likely that a sparger would be used for gas introduction to a surry reactor designed for industrial application, we feel that the maximum interfacial area measured by Calderbank et al. (6) represents a reasonable value.

Values of the mass transfer coefficients were estimated using the correlation proposed by Calderbank and Moo-Young (14) for bubbles smaller than 2.5 mm. Their correlation can be written:

$$k_{L,i} = 3.08[D_{L,i}^2 \rho_L / \mu_L]^{1/3} \qquad (15)$$

Table 4. Solubility Coefficients.

Component	m_i, $\frac{(moles/cm^3)\ g}{(moles/cm^3)}$	Source
H_2	4.35	(22)
CO	3.3	(22)
CO_2	1.77	(22)
CH_4	1.38	(23)
H_2O	1.17	(22)
C_5H_{10}	2.42	(24)

where all quantities are in cgs units. It should be recognized that while this relation was originally developed to describe mass transfer in bubble columns in the absence of solids, it has also been found to be suitable for predicting mass transfer coefficients in slurry reactors (16). Values of the liquid viscosity and gas diffusivities required for the evaluation of $k_{L,i}$ are given in Table 5. The liquid was assumed to be Krupp wax and its density was determined by extrapolation of the data reported by Calderbank et al. (6) to 270°C. The viscosity used was that reported by Bland and Davidson (16) for heavy paraffins.

The diffusivity of H_2 in Krupp was was taken from the experimental data contained in the paper by Calderbank et al. (6). It should be noted that the value for D_{L,H_2} obtained this way is about an order of magnitude greater than that obtained from the Wilke-Chang correlation (17) and used in the calculations carried out by Satterfield and Huff (9), and Deckwer et al. (9). The diffusivity for CO in Krupp wax was obtained from experimental data reported in the paper by Zaidi et al. (7)

The diffusivities for CH_4 and CO_2 were determined by using the correlation proposed by Hayduk et al. (18). These authors found that the diffusivity for a given component could be described by a constant, characteristic of the diffusing component, multiplied by the liquid viscosity raised to a power. Thus, the diffusivities for CH_4 in Krupp wax at 270°C was taken to be the same as that for CH_4 in hexane at 25°C. Correspondingly, the diffusivity for CO_2 in Krupp wax at 300°C was taken to be equivalent to the diffusivity of CO_2 in heptane at 25°C. A rough estimate of the diffusivity for C_5H_{10} was obtained by extrapolating the data for the diffusivities of CH_4, C_2H_6, and C_3H_8 in hexane at 25°C to higher carbon numbers. The diffusivity of H_2O estimated from that of CH_4 using the dependence of diffusivity on specific volume proposed by Reddy and Doraiswamy (21).

For the purpose of illustrating the effects of mass transfer on the liquid phase concentrations of H_2 and CO, it was assumed that the reaction stoichiometry could be represented by

$$2H_2 + 2CO \rightleftharpoons CH_4 + CO_2$$

This implies that CH_4 is the major synthesis product and that the catalyst exhibits a high water-gas-shift activity. The Damkohler number was taken to be 7.15, so as to achieve a 70 percent conversion of carbon monoxide for a gas space time of 70 s. The selected relationship between space time and conversion is representative of that found experimentally by Kölbel et al. (3), working with an iron catalyst at 270°C.

β) Numerical Methods

Equations 8-10 and 13, together with the boundary conditions given by Eq. 3, were solved numerically. The function f_i was defined by adding the right-hand-side of Eq. 13 to its left-hand-side. A zero solution to f_i was then sought by a regula-falsi technique (19). Convergence was accepted when the values of $C_{L,i}$ used to predict new $C_{L,i}$ were within 1 percent.

Table 5. Diffusivities and Viscosity Used to Estimate $k_{L,i}$.

Parameter		Source
μ,cp	0.33	(16)
D_{CO}, cm^2/sec	0.324×10^{-4}	(17)
D_{H_2}, cm^2/sec	12.0×10^{-4}	(6)
D_{CO_2}, cm^2/sec	0.6×10^{-4}	(17)
C_{H_2O}, cm^2/sec	1.24×10^{-4}	(20)
D_{CH_4}, cm^2/sec	0.9×10^{-4}	(18)
$D_{C_5H_{10}}$, cm^2/sec	0.5×10^{-4}	(18)

c) Results and Discussion

Figure 11 illustrates the axial concentration profiles for each component in both the gas and liquid phases, for the case in which τ_G = 70 s and τ_L = 700 s. The difference in the shapes of the gas-phase profiles for H_2 and CO, and for CH_4 and CO_2, as well as the relative concentrations of each component in the liquid phase are directly related to the magnitude of the mass-transfer coefficient associated with each component. Because the mass-transfer coefficient for H_2 is large relative to that for CO (see Table 5), the gas-phase concentration of H_2 drops off more rapidly than that of CO near the column entrance. The gas-phase profiles predicted for CH_4 and CO_2 can be explained in a similar manner. Both products are produced at an identical rate; however, because the mass-transfer coefficient for CH_4 is larger than that for CO_2, the gas-phase concentration for CH_4 exceeds that for CO_2 over a major portion of the column height. The flattening out of the H_2, CO_2 and CH_4 profiles for $\zeta \geq 0.4$, is indicative of an approach to gas-liquid equilibrium for these components. It is interesting to note that Θ_{G,CH_4} and Θ_{G,CO_2} exceed their $\Theta_{i,L}$ for $\zeta \geq 0.48$. This is due to the depletion of CO from the gas phase in the upper portion of the column. The most slowly transfered component, CO, does not achieve equilibrium before reaching the column exit.

An important consequence of the difference in the mass-transfer rates of different components is that the H_2/CO ratio in the liquid phase is greater than that in the gas feed. This results directly from the fact that while the fluxes of CO and H_2 to the surface of the catalyst particles are identical, the liquid-phase gradient for H_2 is much smaller than that for CO.

The influence of a reduction in the gas-phase space time to 35 s is shown in Fig. 12. In performing the calculations shown in this figure, it was assumed that both ε_G and a are independent of gas velocity. This assumption is supported by the experimental observations reported by Calderbank et al. (6) for $\mu_G > 4$ cm-sec^{-1}. As a result of the lower space time, the gas-phase concentrations presented in Fig. 12 change more slowly with than those shown in Fig. 10, but otherwise the trends observed in both figures are qualitatively the same. Comparison of the liquid-phase H_2/CO ratio for the two gas-phase space velocities shows that the ratio is higher for the lower space velocity. Thus, C_L, H_2/C_L,CO = 2.75 for τ_G = 35 s, and C_L,H_2/C_L,CO = 1.68 for $_G$ = 70 s. This difference can be explained in terms of the differences in the gas-phase concentration profiles for the two cases. For τ_G = 35 s, the gas-phase concentrations for H_2 and CO deviate to a lesser degree than for τ_G = 70 s. As a consequence, the liquid-phase concentrations of H_2 and CO must differ by a more significant degree for the lower space velocity, in order to maintain the required relative driving forces for mass transfer through the liquid phase. For τ_G = 70 s, the average CO concentration in the gas phase is much higher than the average H_2 concentration, and the liquid phase concentrations of H_2 and CO need not differ by as much to satisfy the liquid-phase mass balance.

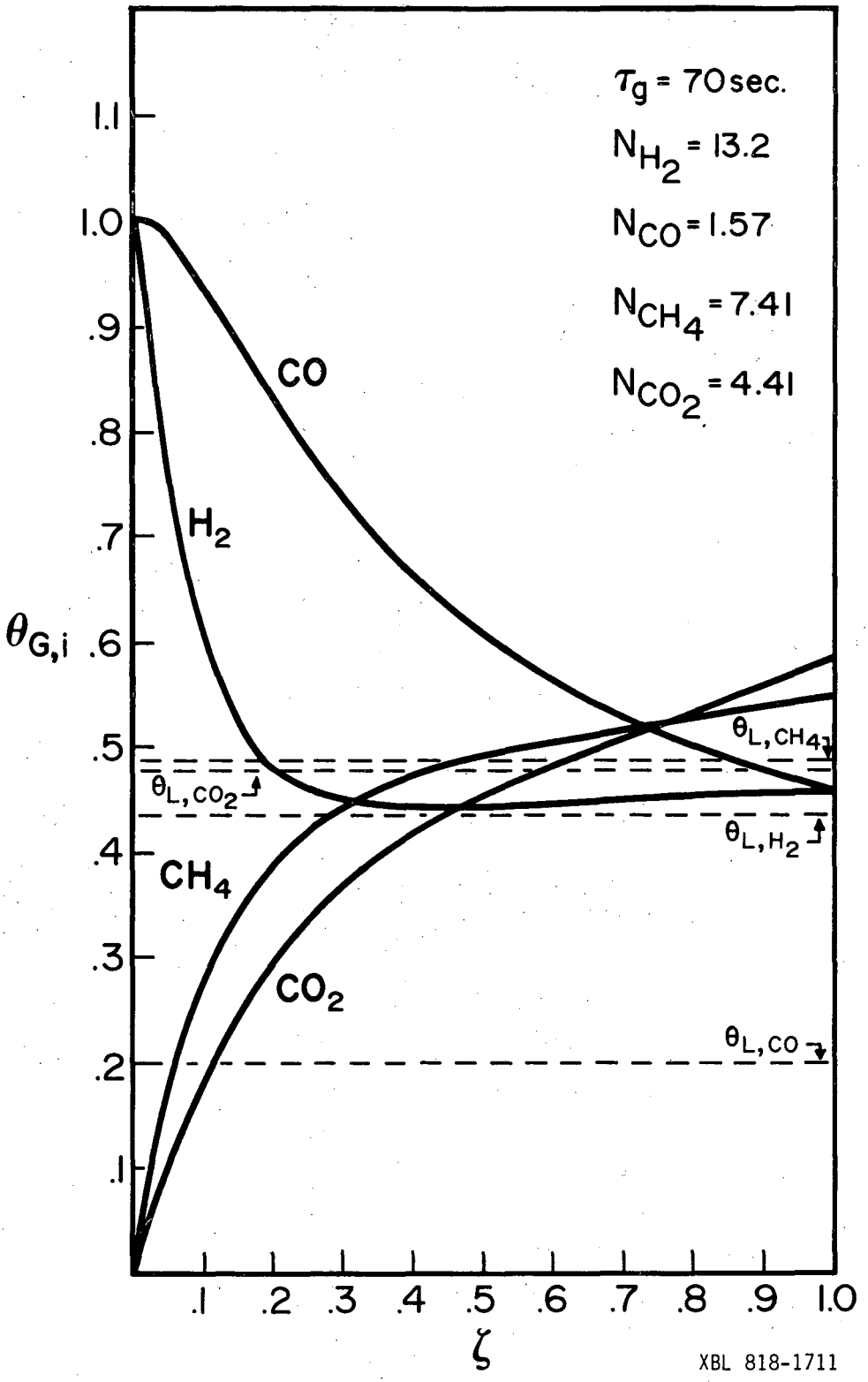
τ_g = 70 sec.
N_{H_2} = 13.2
N_{CO} = 1.57
N_{CH_4} = 7.41
N_{CO_2} = 4.41
CO
H_2
CH_4
CO_2
θ_{L,CH_4}
θ_{L,CO_2}
θ_{L,H_2}
$\theta_{L,CO}$
$\theta_{G,i}$
1.1
1.0
.9
.8
.7
.6
.5
.4
.3
.2
.1
.1 .2 .3 .4 .5 .6 .7 .8 .9 1.0
ζ
XBL 818-1711

Figure 11

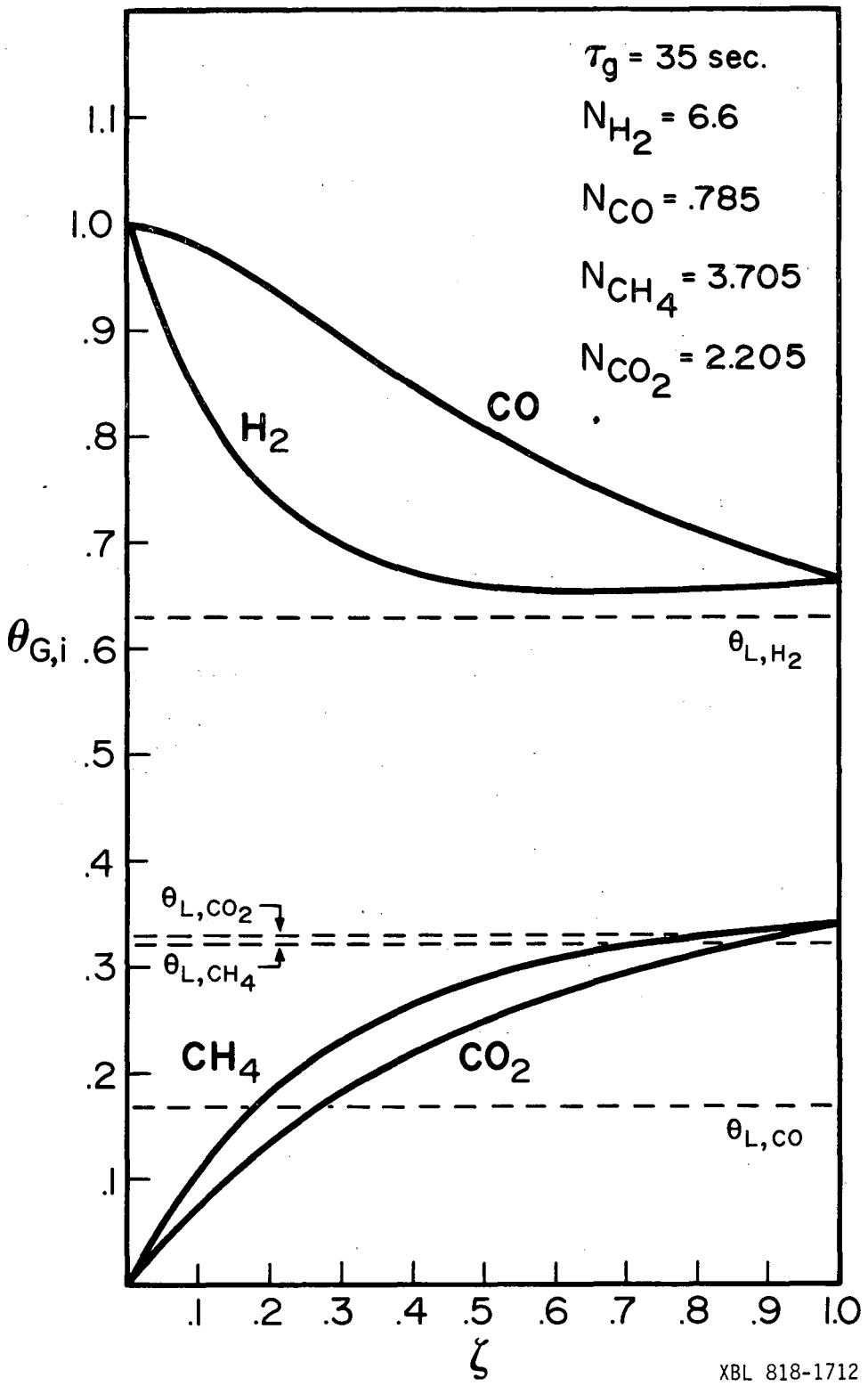
τ_g = 35 sec.
N_{H_2} = 6.6
N_{CO} = .785
N_{CH_4} = 3.705
N_{CO_2} = 2.205
CO
H_2
$\theta_{G,i}$
θ_{L,H_2}
θ_{L,CO_2}
θ_{L,CH_4}
CH_4
CO_2
$\theta_{L,CO}$
1.1
1.0
.9
.8
.7
.6
.5
.4
.3
.2
.1
.1 .2 .3 .4 .5 .6 .7 .8 .9 1.0
ζ
XBL 818-1712

Figure 12

The extent to which the H_2/CO ratio in the liquid phase exceeds that fed to the column in the gas phase is a strong function of the relative magnitudes of k_{L,H_2} and $k_{L,CO}$, as shown in Fig. 13. The two curves shown in this figure were generated by varying the k_{L,H_2}, holding $k_{L,CO}$ and all other parameters constant. The H_2/CO ratio at $N_{H_2} = N_{CO}$ depends on the feed H_2/CO ratio as well as the ratio of H_2 to CO consumption during synthesis. For the case under consideration, both the feed ratio and the consumption ratio are unity and, hence, the liquid-phase H_2/CO ratio becomes 0.76, the ratio of the solubilities. As the value of N_{H_2}/N_{CO} increases above unity, the H_2/CO ratio in the liquid phase rises rapidly and then passes through a broad maximum. This trend, which is different for each value of τ_g, can be explained in terms of the effect of increasing k_{L,H_2} on the axial-concentration profiles for H_2 and CO. As $k_{L,H_2}/k_{L,CO}$ increases, the H_2 profile falls progressively below that for CO, as a consequence of the increased rate of H_2 mass transfer. This causes the liquid-phase concentration of H_2 to rise above that for CO. Eventually, the liquid-phase H_2 concentration rises to the point where it is in equilibrium with the exiting gas phase concentration. Further increase in k_{L,H_2} relative to $k_{L,CO}$ beyond this point does not cause a further increase in Θ_{L,H_2} but results only in a greater and greater proportion of the gas phase coming into equilibrium with the liquid-phase H_2 concentration. This effect can be seen by comparing Figs. 11 and 14, and also Figs. 12 and 15. Examination of these figures also shows that the more rapid transfer of H_2 into the liquid phase causes the gas-phase concentration of CO to rise and this, in turn, causes a further transfer of CO into the liquid. The net result is a slight increase in liquid-phase concentration of CO. It is this latter effect which is responsible for the decrease in $C_{L,H_2}/C_{L,CO}$ seen in Fig. 13 for high values of $N_{L,H_2}/N_{L,CO}$.

The extent to which gas-liquid mass transfer influences $\Theta_{L,H_2}/\Theta_{L,CO}$ strongly depends on the magnitudes of a and Da, as shown in Figs. 16 and 17. In Fig. 16 it is seen that as a decreases, the H_2/CO ratio rapidly increases above that in the feed, i.e., 1:1. Mass transfer effects also become more pronounced as the Damkohler number increases. Figure 17 shows that $\Theta_{L,H_2}/\Theta_{L,CO}$ increases dramatically with increasing values of Da.

The influence of the ratio of the solubility constants for H_2 and CO on the H_2/CO ratio in the liquid phase is shown in Fig. 18. The solid line traces the effects of m_{H_2}/m_{CO} on $C_{L,H_2}/C_{L,CO}$ in the presence of mass transfer effects, and the dashed line indicates what would occur in the absence of any mass-transfer limitations. It is apparent that as the solubility of H_2 relativ to CO increases (i.e., m_{CO}/m_{H_2}), mass-transfer effects have an increasingly larger affect on the liquidphase ratio of H_2 to CO. An explanation for this trend can be deduced from Eqs. 1 and 13. It is apparent from Eq. 1 that a decrease in m_{H_2} causes an increase in the driving force for H_2 mass transfer. From Eq. 13, it can be seen that Θ_{L,H_2} determines the rate of hydrogen mass transfer, while the quality $\Theta_{L,H_2}/m_{H_2}$ determines the rate of reaction.

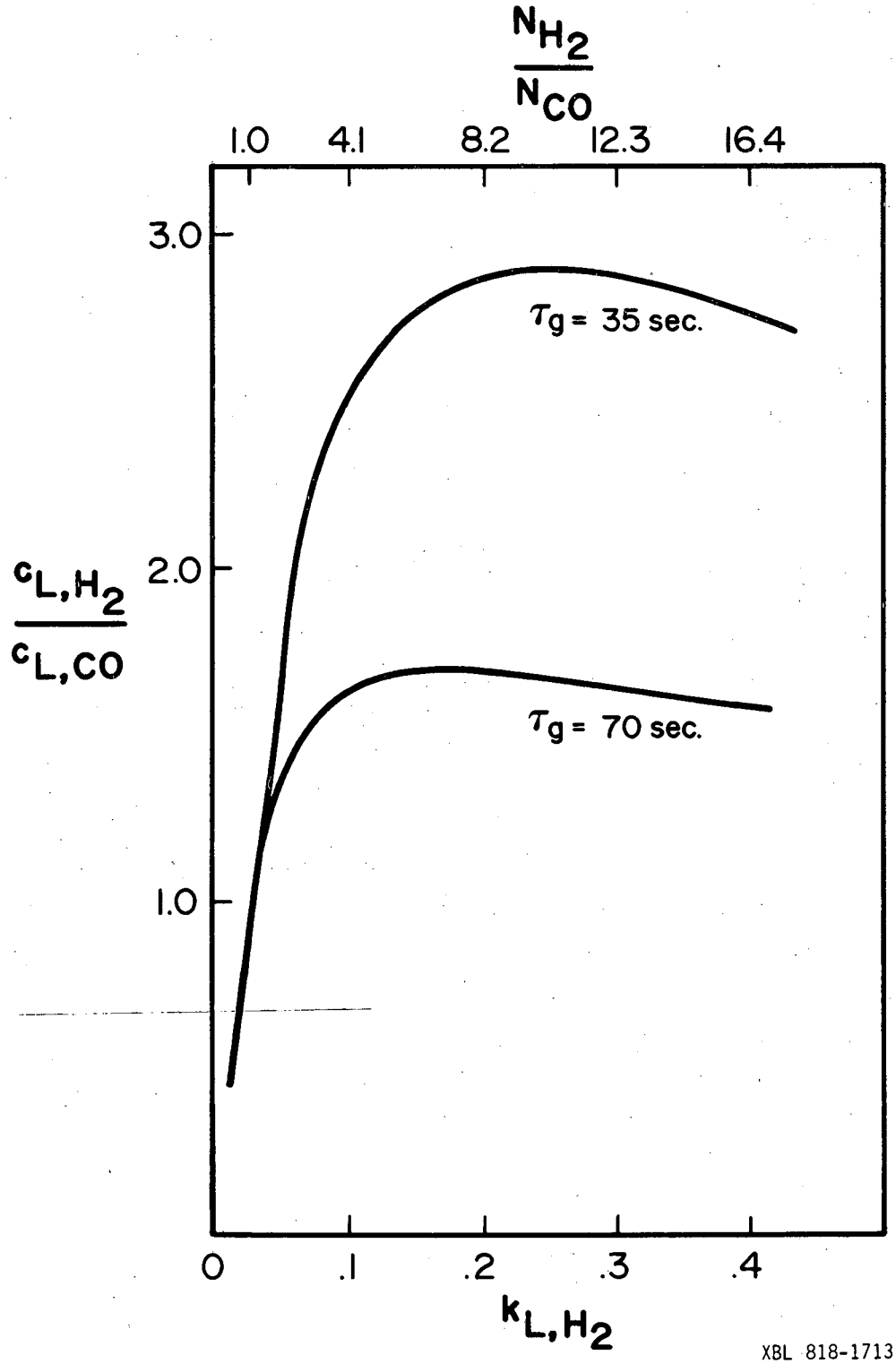
$\frac{N_{H_2}}{N_{CO}}$
1.0
4.1
8.2
12.3
16.4
3.0
2.0
1.0
$\frac{c_{L,H_2}}{c_{L,CO}}$
τ_g = 35 sec.
τ_g = 70 sec.
0
.1
.2
.3
.4
k_{L,H_2}
XBL 818-1713

Figure 13

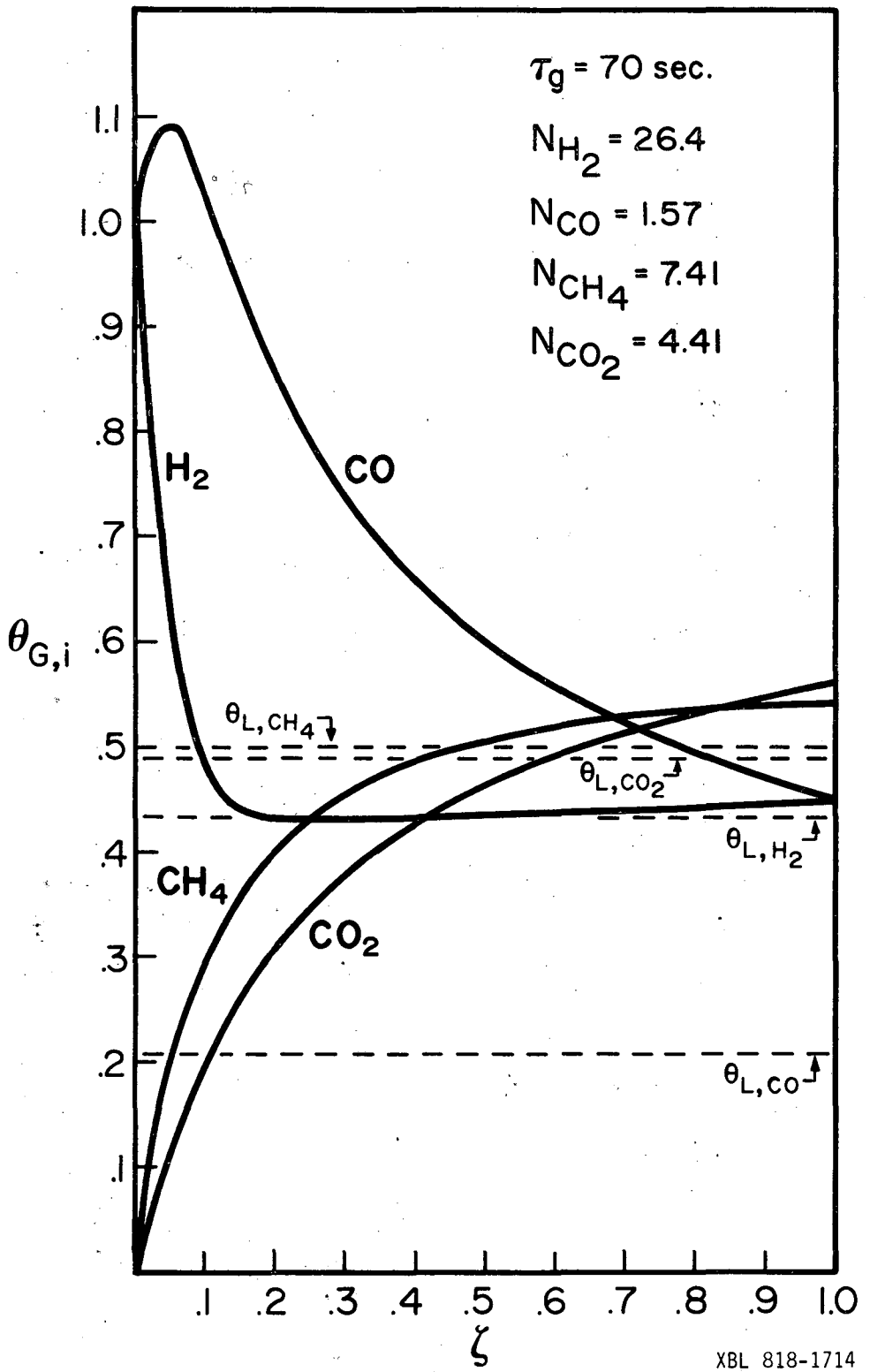
τ_g = 70 sec.
N_{H_2} = 26.4
N_{CO} = 1.57
N_{CH_4} = 7.41
N_{CO_2} = 4.41
$\theta_{G,i}$
H_2
CO
CH_4
CO_2
θ_{L,CH_4}
θ_{L,CO_2}
θ_{L,H_2}
$\theta_{L,CO}$
1.1
1.0
.9
.8
.7
.6
.5
.4
.3
.2
.1
.1 .2 .3 .4 .5 .6 .7 .8 .9 1.0
ζ
XBL 818-1714

Figure 14

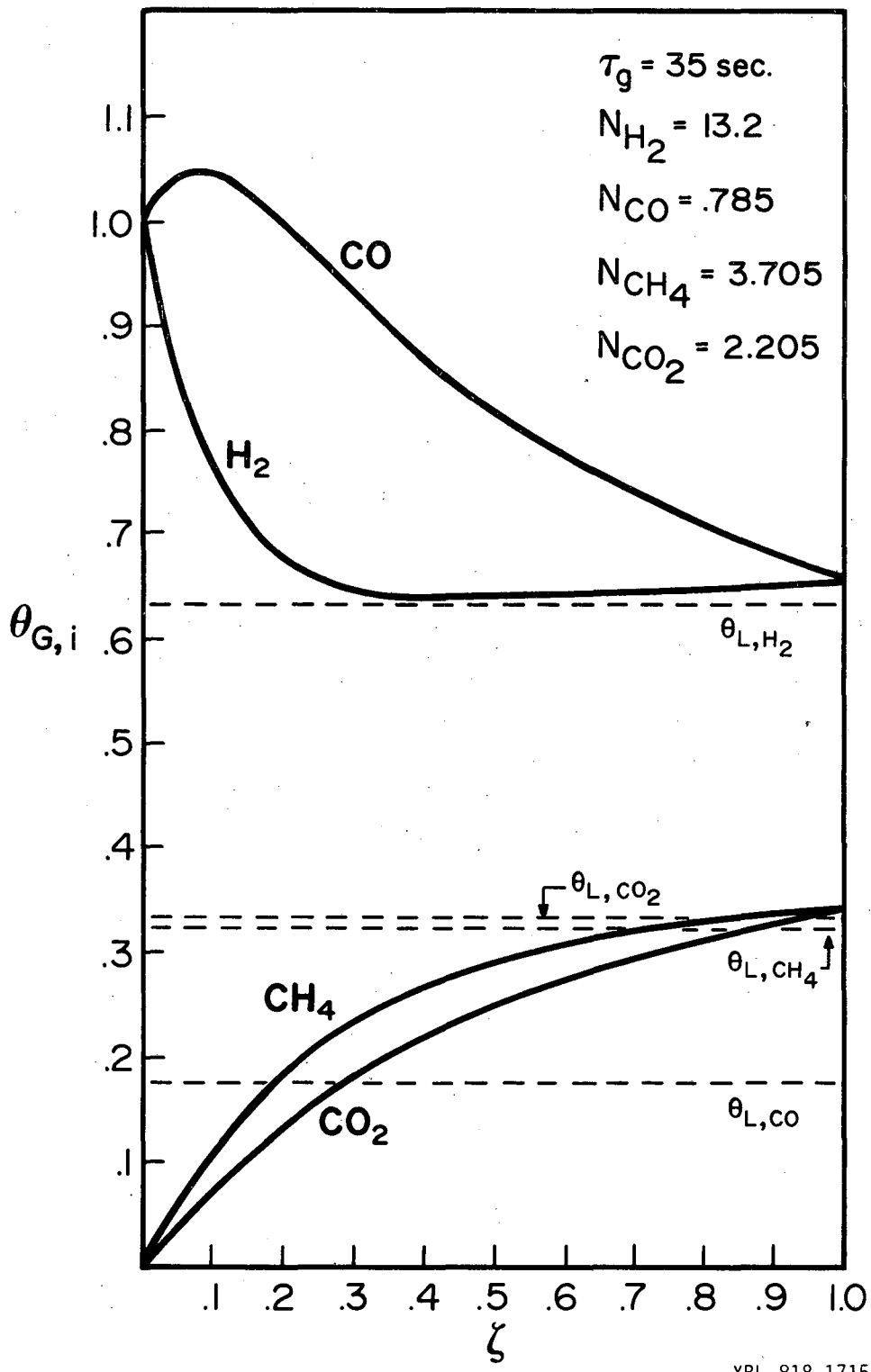

XBL 818-1715

Figure 15

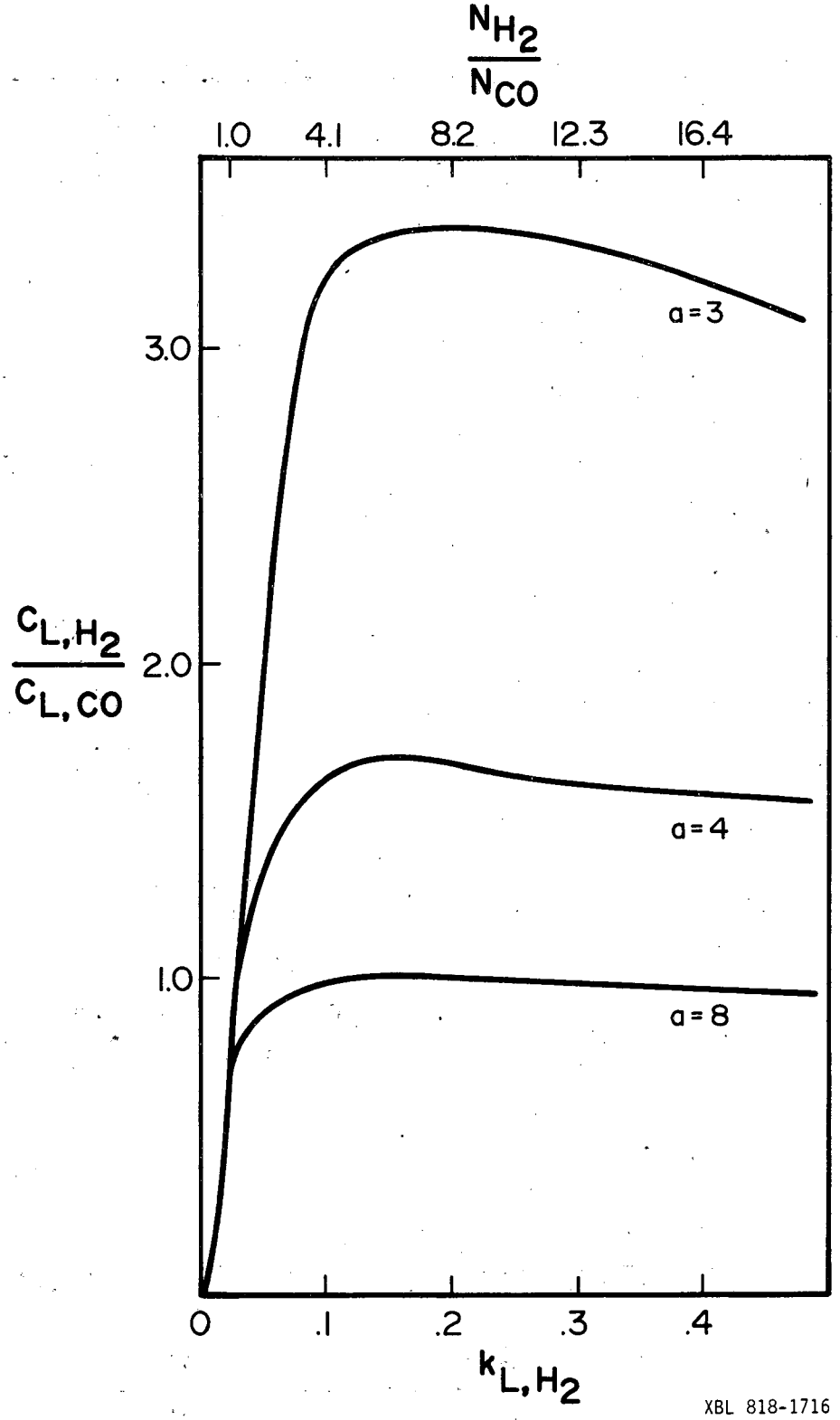
$\frac{N_{H_2}}{N_{CO}}$
1.0
4.1
8.2
12.3
16.4
a=3
a=4
a=8
3.0
2.0
1.0
$\frac{C_{L,H_2}}{C_{L,CO}}$
0
.1
.2
.3
.4
k_{L,H_2}
XBL 818-1716

Figure 16

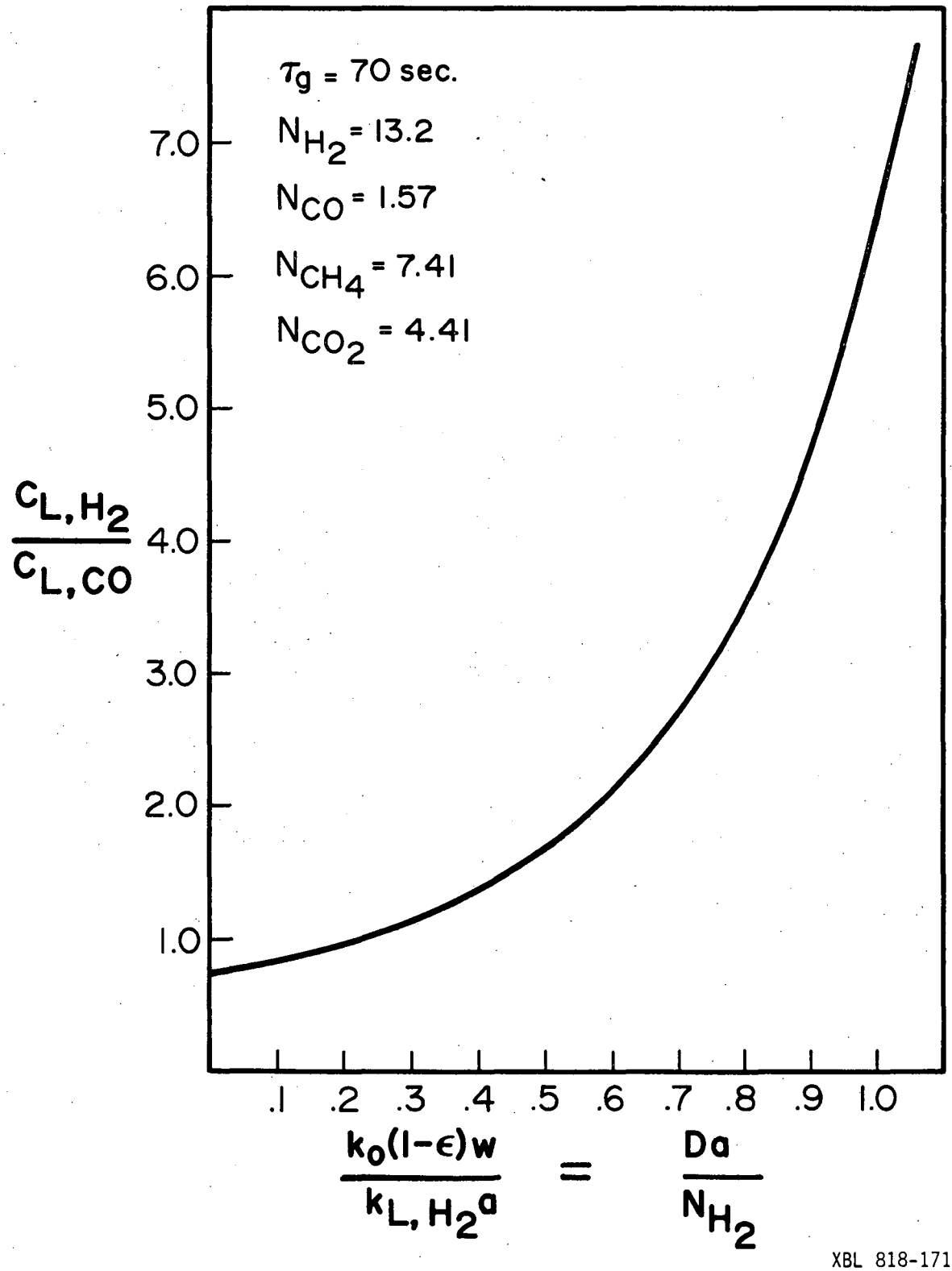

XBL 818-1717

Figure 17

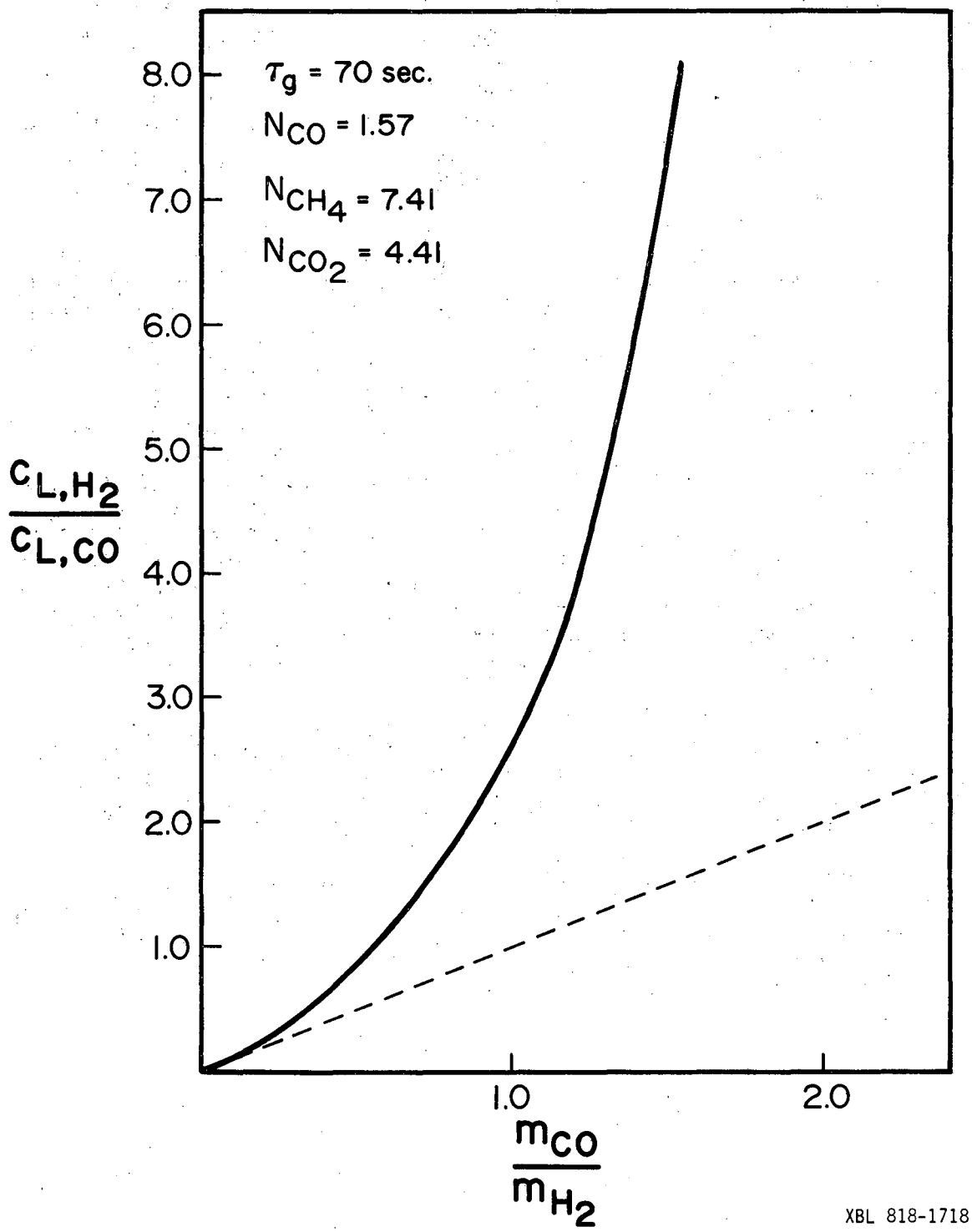

XBL 818-1718

Figure 18

Thus, for a given Θ_{L,H_2}, decreasing m_{H_2} increases the rate of reaction while the rate of hydrogen mass transfer remains constant. As m_{H_2} decreases, the driving forces for both hydrogen and carbon monoxide transfer must increase. The driving force for transfer of hydrogen, however, increases by virtue of its increased solubility, while the driving force for transfer of carbon monoxide can be increased only by lowering its liquid concentration.

The stoichiometric relationship between the rates of H_2 and CO consumption depends upon the nature of the products produced. In the example considered thus far, it has been assumed that CH_4 and CO_2 are the principle products and, hence, that equivalent quantities of H_2 and CO are consumed. If, on the other hand, one considers that olefins and CO_2 are the primary products, then twice as much CO as H_2 will be consumed. Figure 19 shows the effects of k_L,H_2 on $C_{L,H_2}/C_{L,CO}$ for the case in which pentene is taken as a typical olefin product. It is apparent that the H_2/CO ratio in the liquid phase can be substantially greater than the ratio in the feed gas, 0.67, and that the maximum enhancement in the liquid-phase H_2/CO ratio is greater in this case than in the case where CH_4 is the primary hydrocarbon product (see Fig. 11). Both of these observations are a direct result of the fact that the consumption of CO exceeds the consumption of H_2. It is interesting to note that the liquid H_2/CO ratio does not go through a maximum as k_L,H_2 increases. Since the feed concentration of carbon monoxide is high, changes in the gas phase CO concentration profile have only a small effect on the driving force for transfer of carbon monoxide.

If the consumption of H_2 exceeds the consumption of CO, then the H_2/CO ratio in the liquid-phase falls below that in the feed gas. This situation is shown in Figs. 20 and 21 for the case in which CH_4 and H_2O are considered to be primary products, a situation which would arise if the catalyst had no water-gas-shift activity (25).

The influence of mass-transfer limitations on the productivity of a slurry reactor can be examined in terms of a column effectiveness factor, η. This characteristic describes the ratio of the actual rate of reaction to that occurring in the absence of any mass transfer limitations. Thus,

$$\eta = r_i/r_i^{max}$$

$$= \Theta_{L,H_2}/\Theta_{L,H_2}^{max} \qquad (16)$$

When the rate of mass transfer for all components becomes very high, the inlet gas will instantaneously equilibrate with the liquid. Since the liquid-phase concentrations are assumed to be independent of axial position, the gas-phase composition is constrained to a constant value throughout the column, namely the exit concentration. Under these

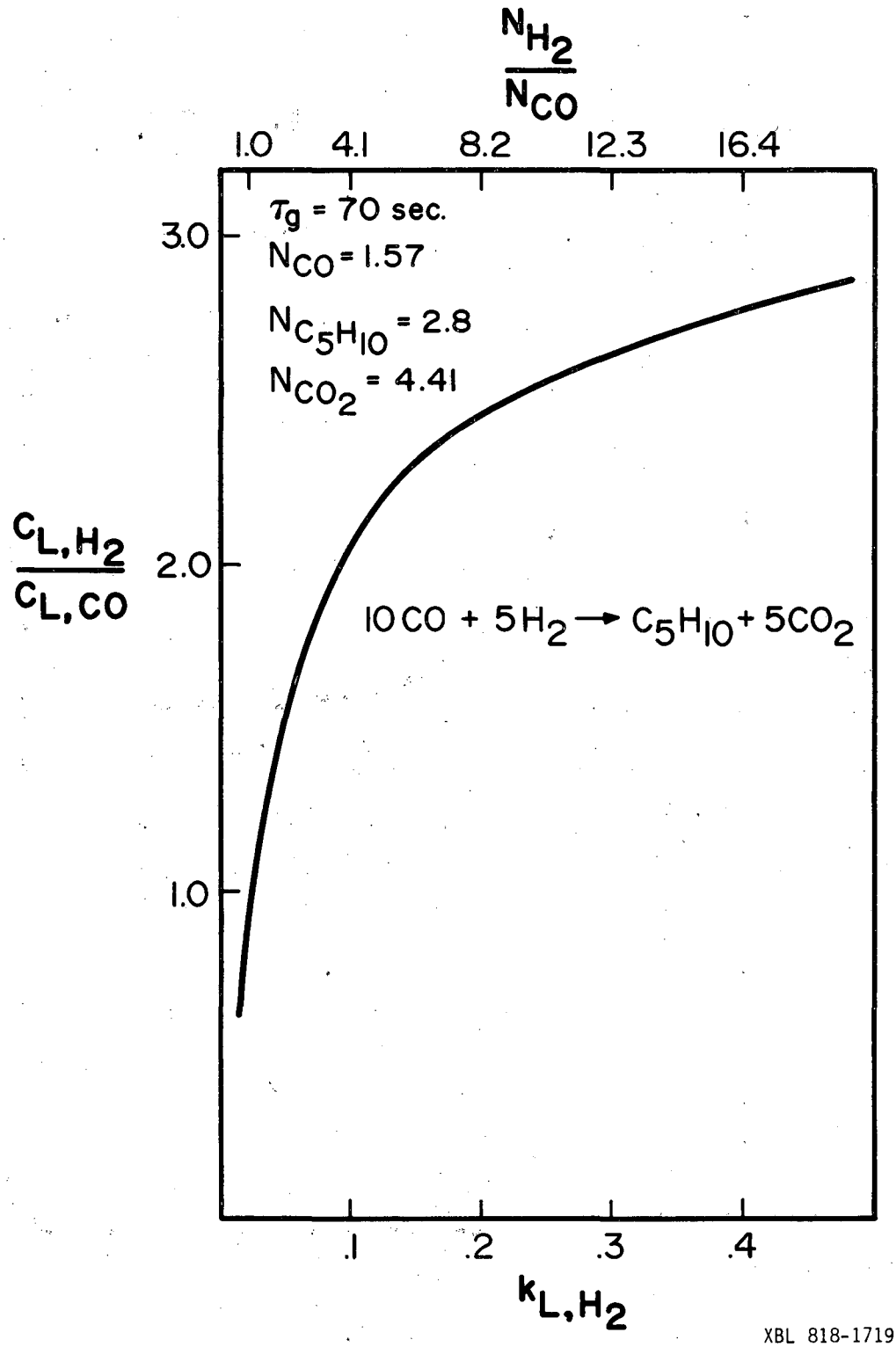

XBL 818-1719

Figure 19

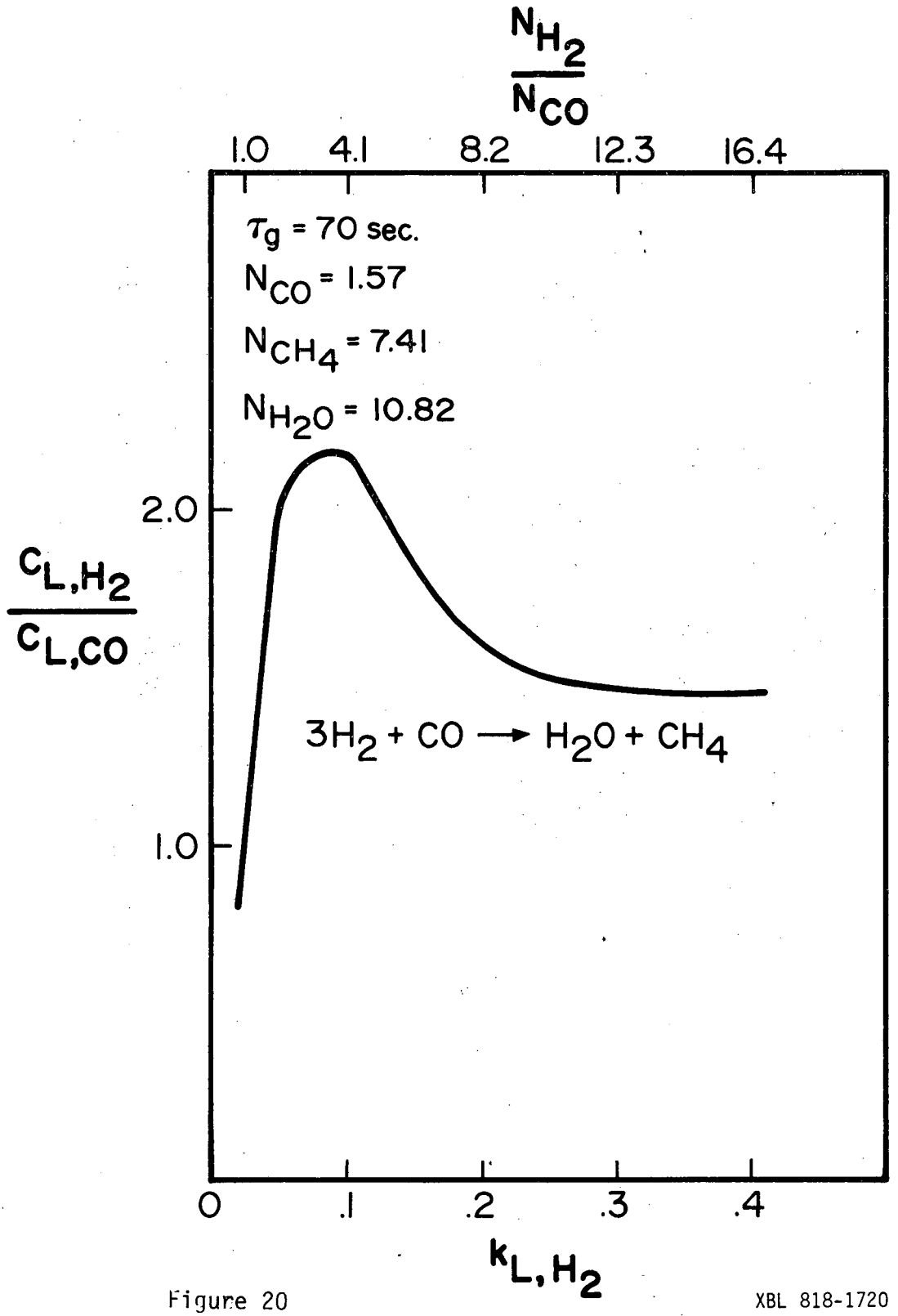

Figure 20

XBL 818-1720

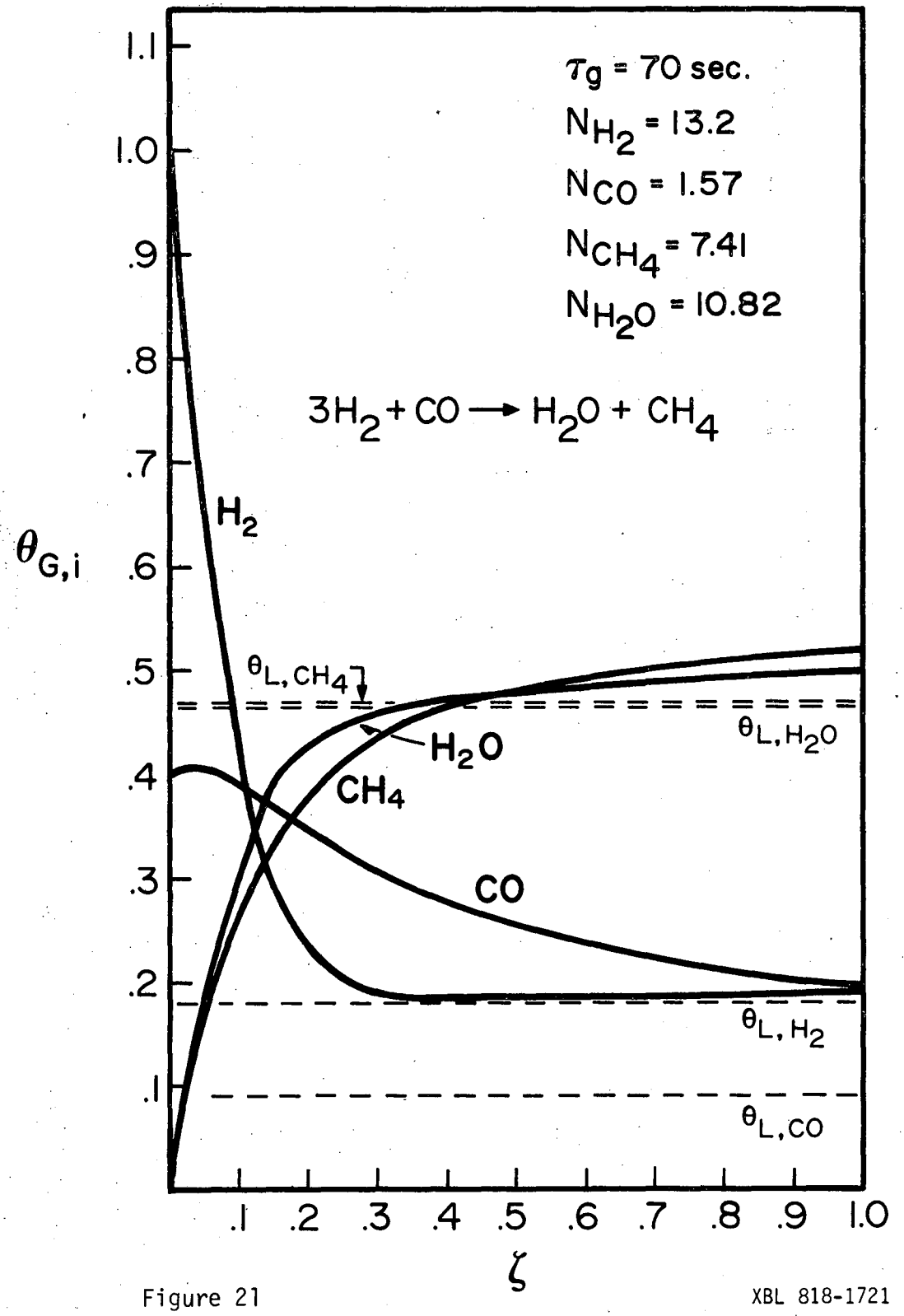

Figure 21

XBL 818-1721

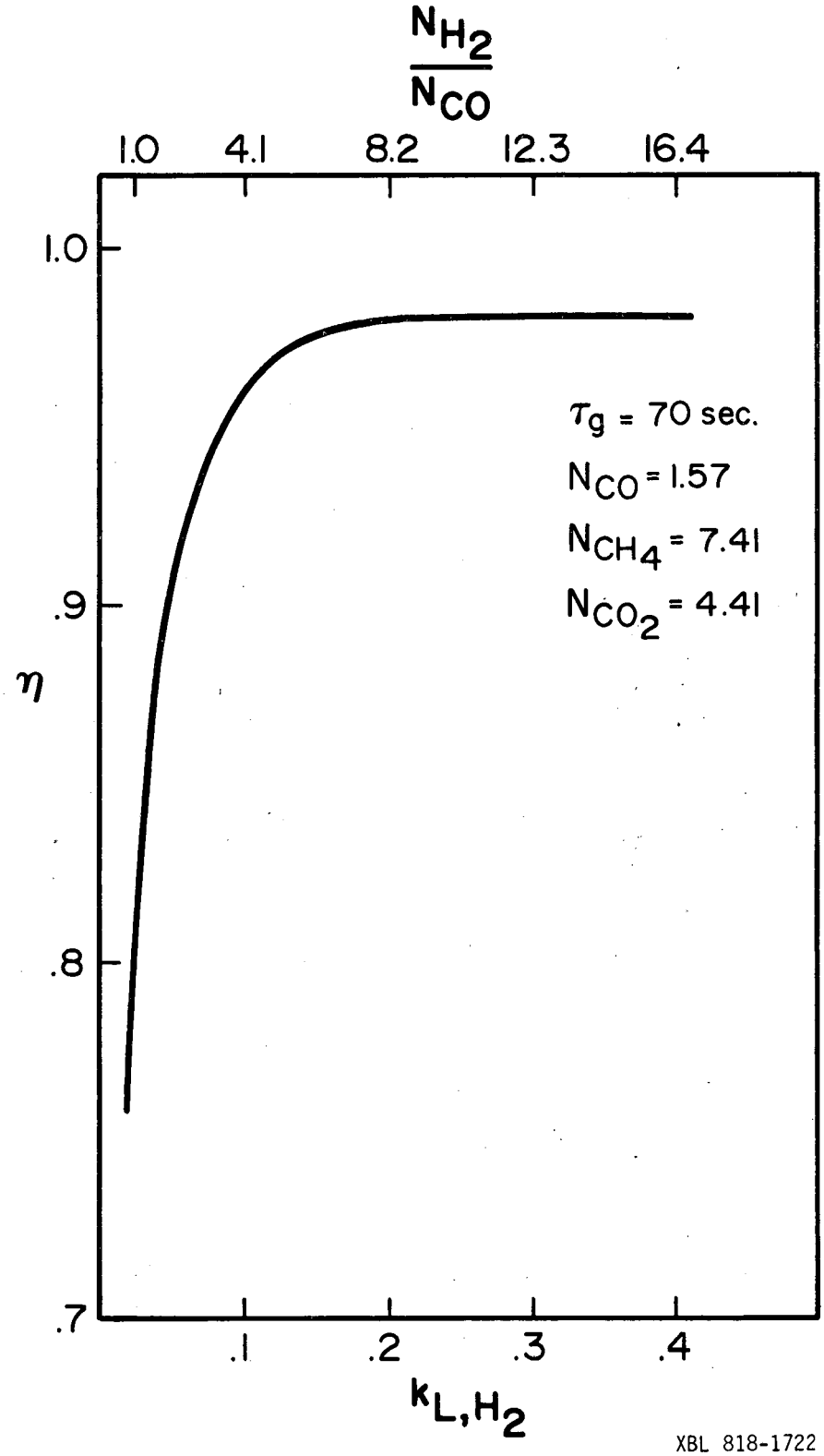

XBL 818-1722

Figure 22

conditions, the component mass balances are represented by algebraic equations of the following form

$$Q_L C_{L,i}^{max} + V_r \nu_i w(1 - \varepsilon_G)\, k_o C_{L,H_2}^{max} = Q_G^o C_{G,i}^o - Q_G C_{G,i}^{max} \quad . \tag{17}$$

Since the gas and liquid are at equilibrium,

$$C_{L,i}^{max} = C_{G,i}^{max}/m_i \quad . \tag{18}$$

Introduction of Eq. 18 into Eq. 17 and nondimensionalization of the resulting equation, using the definitions given in Eq. 7, gives

$$\theta_{G,i}^{max} + \nu_i Da \frac{\tau_L}{\tau_G} \frac{m_i}{m_{H_2}} \theta_{G,H_2}^{max} = m_i \frac{\tau_L}{\tau_G} (\theta_{G,i}^o - \upsilon \theta_{G,i}^{max}) \tag{19}$$

In addition to Eq. 19, one must also take into account an overall mass balance given in nondimensional form by

$$\sum_{i=1}^{n} (\theta_{G,i}^{max}/m_i) + Da \frac{\tau_L}{\tau_G m_{H_2}} \theta_{G,H_2}^{max} \sum_{i=1}^{n} \nu_i = \frac{\tau_L}{\tau_G} \theta_G (1 - \upsilon) \tag{20}$$

Values for $\theta_{G,i}^{max}$ are obtained by the simultaneous solution of Eqs. 20 and 21. For the parameter values listed in Tables 4 and 5, it was determined that $\theta_{L,H_2}^{max} = 0.44$. This value was then used in Eq. 16 to determine η as a function N_{H_2}, all other parameters being held constant. Figure 22 shows that for the parameters used in the calculations illustrated in Fig. 13, the value of η is always in excess of 0.76. This indicates that for the chosen conditions mass-transfer has only a very modest influence on the overall reactor productivity. Figure 13 shows, however, that even this limited degree of mass-transfer limitation has a profound affect on the H_2/CO ratio in the liquid phase.

iii) Conclusions

The present analysis has shown that the H_2/CO ratio in the liquid phase of a slurry reactor used for Fischer-Tropsch synthesis is a sensitive function of differences in the solubilities and mass-transfer coefficients for H_2 and CO, and that the liquid-phase H_2/CO ratio can differ substantially from that of the gas fed to the reactor. In addition to the factors mentioned, the direction and magnitude of the change in liquid-phase H_2/CO ratio is dependent on the H_2-CO consumption ratio, the interfacial area, the Damkohler number, and the space velocity of the feed gas. It has been demonstrated that the influence of mass-transfer effects on the liquid-phase

H_2/CO ratio can be larger even under circumstances where the gas-liquid mass-transfer resistance is a relatively small fraction of the overall reaction resistance. Since the liquid-phase H_2/CO ratio influences the average molecular weight of the products formed, the olefin to paraffin ratio of the products, and the formation of free carbon, knowledge of the dependence of the H_2/CO ratio on reaction conditions should be taken into account in the design of slurry columns used for Fischer-Tropsch systhesis.

iv) References

1. Newsome, D. S., Catalysis Review, Sci. Eng. 21, 275-318 (1980).
2. McKee, W. G., M. S. Thesis, University of California, Berkeley, Department of Chemical Engineering (1980).
3. Kölbel, H., and Ralek, M., Cat. Rev. 21, 225 (1980).
4. Statterfield, C., Mass Transfer in Heterogeneous Catalysis, MIT Press, 1970.
5. Cannella, W. and Bell, A. T., unpublished results.
6. Calderbank, P. H., Evans, F., Farley, R., Jepson, G., and Poll, A., Catalysis in Practice, London, Instn. Chem. Engrs. (1963).
7. Zaidi, A., Deckwer, W. D., Louisi, Y. and Ralek, M., Ger. Chem. Engr. 2, 94 (1979).
8. Satterfield, C. and Huff, G., Chem. Eng. Sci. 35, 195 (1980).
9. Deckwer, W. D., Serpemen, Y., Ralek, M., and Schmidt, B., Chem. Eng. Sci. 36, 765 (1981).
10. Satterfield, C. and Huff, G., Chem. Eng. Sci. 36, 790 (1981).
11. Deckwer, W. D., Serpemen, Y., Ralek, M. and Schmidt, B., Chem. Eng. Sci. 36, 791 (1981).
12. Dry, M. E., Ind. Eng. Chem. Prod. Res. Develop. 15, 282 (1976).
13. Zien el Deen, A., Jacobs, J. and Baerns, M., Chemical Reaction Engineering Symposium, ACS (Houston), 1978.
14. Calderbank, P. H. and Moo-Young, M. B., Chem. Eng. Sci. 16, 39 (1961).
15. Chaudhari, R. V. and Ramachandran, P. A., AIChE J. 26, 177 (1980).
16. Bland, W. and Davidson, R. L., Petroleum Processing Handbook, McGraw-Hill.

17. Sherwood, T., Rigford, R. and Wilke, C., Mass Transfer, McGraw Hill (1975).

18. Hayduk, W., Castraneda, R., Bromfield, H. and Perras, R., AIChE J. 19, 859 (1973).

19. Lapidus, L., Digital Computation for Chemical Engineers, McGraw Hill (1962).

20. Reddy, K. and Doraiswamy, Ind. Eng. Chem. Fundam. 6, 77 (1967).

21. Peter, S. and Weinert, M., Z. Physik Chem. 5, 114 (1955).

22. Battino, R. and Wilhelm, E., Chem. Rev. 73, 7 (1973).

23. Hayoluk, W. and Chen, S., Can. J. Chem. Eng. 48, 93 (1970).

24. Pichler, H., "Twenty-Five Years of Synthesis of Gasoline by Catalytic Conversion of Carbon Monoxide and Hydrogen," Advances in Catalysis 4, Academic Press, NY, 1952.

This report was done with support from the Department of Energy. Any conclusions or opinions expressed in this report represent solely those of the author(s) and not necessarily those of The Regents of the University of California, the Lawrence Berkeley Laboratory or the Department of Energy.

Reference to a company or product name does not imply approval or recommendation of the product by the University of California or the U.S. Department of Energy to the exclusion of others that may be suitable.

TECHNICAL INFORMATION DEPARTMENT
LAWRENCE BERKELEY LABORATORY
UNIVERSITY OF CALIFORNIA
BERKELEY, CALIFORNIA 94720